Nano Research

ISSN 1998-0124 CN 11-5974/O4
https://doi.org/10.26599/NR.2026.94909335

Review Article

Engineering advanced sensors for monitoring physiological responses in microphysiological systems

Minseung Shin[1], Jun Sang Choi[2], Nayeong Kang[2], Song Ih Ahn[2](✉)

[1] School of Mechanical Engineering, Pusan National University, Busan 46241, Republic of Korea

[2] Department of Mechanical Engineering, Korea Advanced Institute of Science and Technology (KAIST), Daejeon 34141, Republic of Korea

Nano Res., **Just Accepted Manuscript** • https://doi.org/10.26599/NR.2026.94909335

https://www.sciopen.com/journal/1998-0124 on Nov. 16, 2026

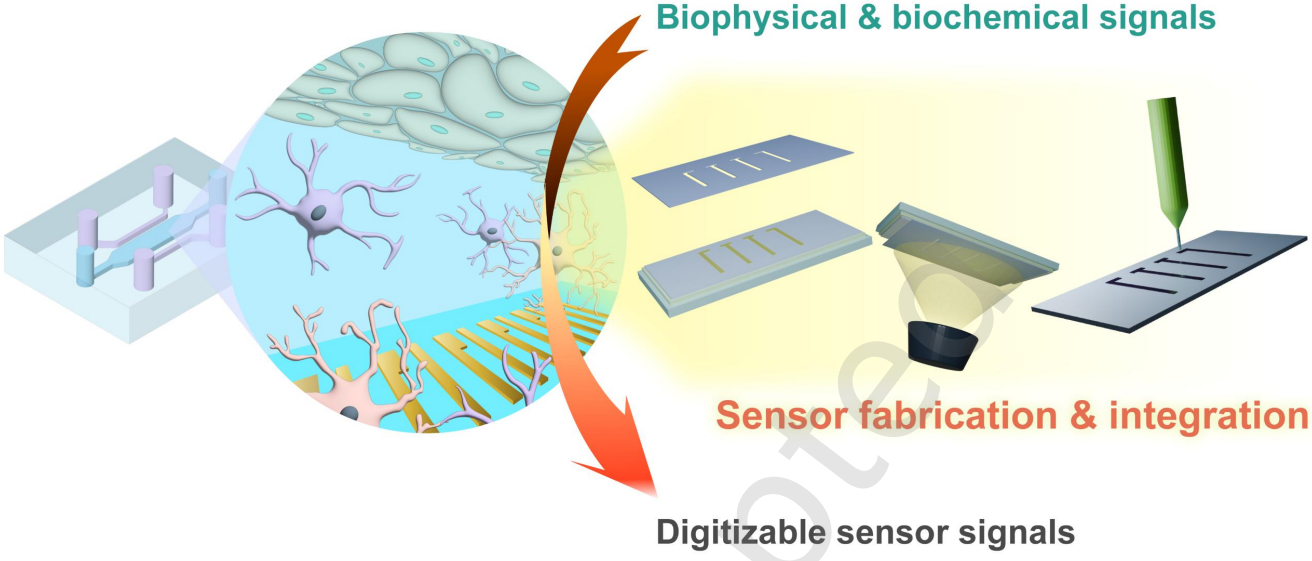
© The Authors(s)

Just Accepted

This is a "Just Accepted" manuscript, which has been examined by the peer-review process and has been accepted for publication. A "Just Accepted" manuscript is published online shortly after its acceptance,which is prior to technical editing and formatting and author proofing. Tsinghua University Press (TUP) provides "Just Accepted" as an optional and free service which allows authors to make their results available to the research community as soon as possible after acceptance. After a manuscript has been technically edited and formatted, and the page proofs have been corrected, it will be removed from the "Just Accepted" web site and published officially with volume and article number (e.g., *Nano Research*, **2025**, *18*, 94906990). Please note that technical editing may introduce minor changes to the manuscript text and/or graphics which may affect the content, and all legal disclaimers that apply to the journal pertain. In no event shall TUP be held responsible for errors or consequences arising from the use of any information contained in these "Just Accepted" manuscripts. To cite this anuscript please use its Digital Object Identifier (DOI®),which is identical for all formats of publication.

Just Accepted

TABLE OF CONTENTS (TOC)



This review discusses sensor integration strategies for reliable monitoring of key physiological signals in microphysiological systems (MPSs). It also summarizes essential considerations for practical implementation, including fabrication method, sensor placement, biocompatibility, signal stability, cost-effectiveness, and AI-assisted design.

Just Accepted

Review Article

Engineering advanced sensors for monitoring physiological responses in microphysiological systems

Minseung Shin [1], Jun Sang Choi [2], Nayeong Kang [2], Song Ih Ahn [2]

[1] School of Mechanical Engineering, Pusan National University, Busan 46241, Republic of Korea
[2] Department of Mechanical Engineering, Korea Advanced Institute of Science and Technology (KAIST), Daejeon 34141, Republic of Korea

Received: 25 June 2026; **Revised: 22 October 2026**; **Accepted: 16 November 2026**

Address correspondence to siahn@kaist.ac.kr

Cite this article: *Nano Research*, 2027, 20, 94909335 https://doi.org/10.26599/NR.2026.94909335

Just Accepted

ABSTRACT: Microphysiological systems (MPSs) have emerged as powerful *in vitro* platforms that recapitulate human microenvironments with high physiological relevance, enabling studies of disease mechanisms, drug responses, and toxicity. Effective use of MPSs requires not only stable maintenance of the engineered microenvironment but also quantitative and continuous monitoring of dynamic physical, chemical, and biological changes over time. While optical methods remain indispensable for visualizing cellular behavior, their limitations in long-term, multi-parameter, and quantitative monitoring have increasingly motivated the integration of sensors directly within MPS. This review focuses on the engineering strategies underlying sensor fabrication and integration in MPSs. We first highlight representative examples of physiological parameters that have been measured using sensor-integrated MPSs. We then summarize recent advances ranging from micro electromechanical system (MEMS)-based microfabrication approaches to emerging additive fabrication techniques, as well as the direct incorporation of commercially available sensors. Key engineering considerations for sensor fabrication and integration are discussed to provide practical guidance for the design of sensor-integrated MPSs. By providing a fabrication- and integration-focused overview of sensor-enabled MPSs, this review aims to inform the rational design of next-generation platforms capable of high-precision, multimodal, and *in situ* biological monitoring. These advances are expected to accelerate the translation of MPS technologies toward more predictive disease models, improved drug screening platforms, and broader applications in translational biomedical research.

KEYWORDS: Microphysiological system (MPS), Organ-on-a-chip, Biosensors, *in vitro* physiological monitoring, Sensor fabrication

Just Accepted

1 Introduction

Understanding the complex physiological and pathological processes that govern human tissues is essential for uncovering disease mechanisms and developing effective therapeutic strategies. Achieving this goal requires experimental platforms that can reproduce key aspects of *in vivo* physiology while remaining accessible to systematic control and quantitative analysis. However, accurately recapitulating the dynamic and multicellular microenvironment of human tissues in controllable experimental platforms has long remained a major challenge.

Early attempts to model human physiology relied mostly on animal models, which have provided invaluable insights but remain limited by interspecies differences, ethical concerns, and translational discrepancies[1, 2]. To address these limitations, conventional *in vitro* culture models have been introduced as simplified alternatives, enabling cost-effective and high-throughput experimentation. However, they fail to recapitulate essential features of native tissues, including multicellular organization, cell–extracellular matrix (ECM) interactions, and spatiotemporally controlled microenvironmental cues[2-4]. These limitations motivated extensive efforts to reconstruct multicellular networks within physiologically relevant microenvironments[3-6].

Microphysiological systems (MPSs), often referred to as an organ-on-a-chip, have emerged as advanced biomimetic microsystems designed to recapitulate key structural and functional features of human tissue physiology under *in vitro* conditions[2, 7]. By integrating microfluidics, tissue engineering, and microfabrication, these systems enable precise control over biochemical gradients, mechanical stimuli, and tissue-tissue interfaces within microscale architectures[8]. MPSs have traditionally been fabricated using soft lithography[9], while recent advances in 3D bioprinting[10, 11], polymer molding techniques[12], and laser micromachining[13] have expanded design flexibility and material choices. These advances have enabled MPSs to recapitulate dynamic in vivo-like microenvironments across diverse tissue and organ systems, including cell–cell interactions, biochemical gradients, and mechanical stimuli. Accordingly, long-term and multi-parameter monitoring is required to capture transient responses, gradual changes, and recovery processes in these dynamic microenvironments[14-17].

To characterize physiological responses within the MPSs, conventional analytical methods such as immunoassays, molecular analyses, and biochemical assays are widely used. Although these approaches provide highly specific and quantitative information, they often require sample collection or tissue harvesting and provide measurements at discrete time points, limiting their ability to capture transient physiological changes[18-23]. Optical imaging, on the other hand, enables visualization of cellular morphology and dynamics[24], but is limited in its ability to provide quantitative, continuous, and multiparameter monitoring[25, 26].

Therefore, integrating sensors capable of real-time, in situ, and label-free measurements is increasingly important for monitoring dynamic physiological responses in MPSs. A variety of sensor-integrated MPS have been explored to monitor key physiological parameters, including barrier integrity[27-29], mechanical properties[30-32], metabolic activity[33] and electrophysiological activity. Several previous reviews have also discussed sensor-integrated MPSs from different perspectives, including sensor technologies and integration[34, 35], microfluidics-based biosensing[36, 37], continuous monitoring[38-40], and biomedical applications[14, 34, 41-43]. While these reviews provide valuable insights into sensing technologies and their applications, the practical implementation of sensor-integrated MPSs remains constrained by several cross-cutting engineering challenges, including long-term measurement reliability, minimally perturbative sensor–tissue integration, multimodal integration, and reproducible and scalable implementation. Building on these previous reviews, the present

review focuses on the engineering considerations that connect physiological monitoring requirements with sensor selection, fabrication and integration strategies, and reliable operation within MPS environments.

In this review, we focus on the engineering considerations that connect physiological monitoring requirements with sensor selection, fabrication and integration strategies, and validation approaches. We first summarize major classes of physiological signals that have been monitored in MPS, including barrier integrity, mechanical responses, physical microenvironmental parameters, metabolic and biochemical microenvironment indicators, and electrophysiological activity. We then review sensor fabrication and integration strategies, including microelectromechanical system (MEMS)-based microfabrication to additive manufacturing and commercial sensor integration, that enable sensor incorporation into MPS. Finally, we discuss key design considerations and practical bottlenecks that currently limit sensor-integrated MPS, including long-term measurement reliability, minimally perturbative sensor–tissue integration, multimodal integration, and reproducible and scalable implementation (**Fig. 1**).

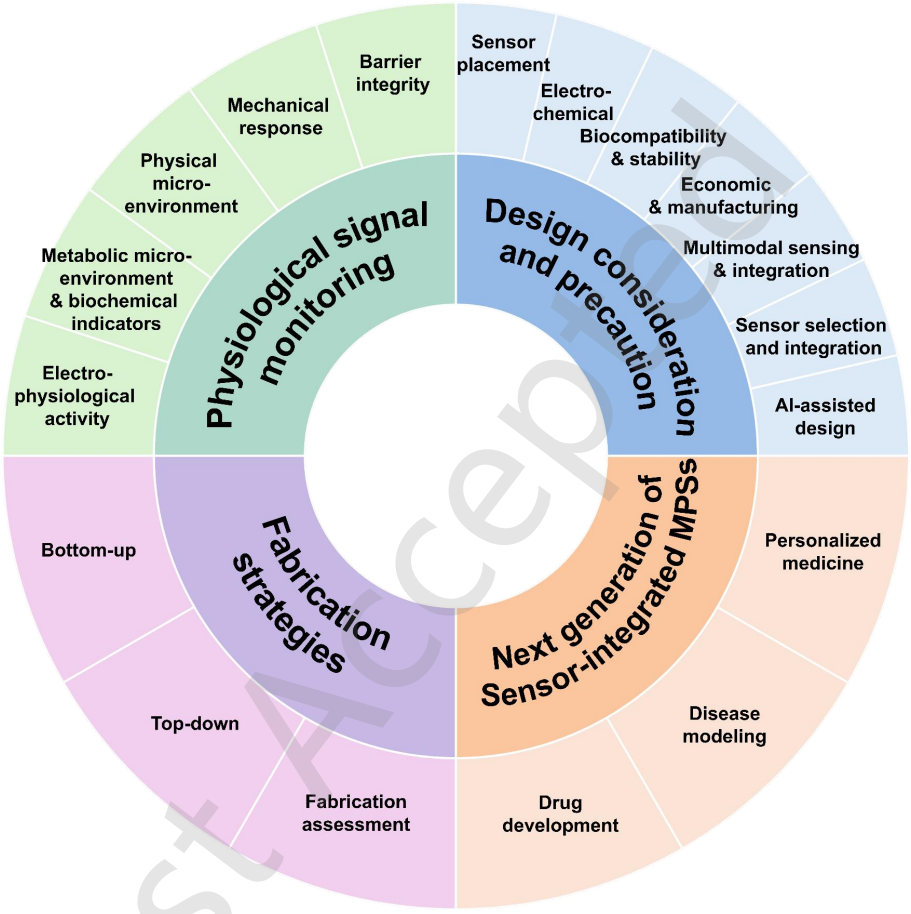


Figure 1 Schematic overview of sensor integrated microphysiological systems (MPSs)

2 Physiological signal monitoring in MPSs

Sensor-integrated MPSs have been developed to monitor diverse physiological signals, including barrier integrity, mechanical responses, physical microenvironmental parameters, metabolic and biochemical indicators, and electrophysiological activity. Because these targets differ in their physiological dynamics and sensing requirements, different sensing principles and measurement strategies are needed. The major sensing approaches, together with their advantages, limitations, and representative MPS applications, are summarized in **Table 1**.

2.1 Barrier integrity

Biological barriers at tissue interfaces play a critical role in regulating selective permeability, maintaining biochemical gradients, and preserving tissue homeostasis[44]. Their dysfunction is closely associated with pathological conditions such as inflammation, infection, and tumor progression[45]. Accordingly, quantitative evaluation of barrier integrity in MPSs is essential to verify the formation of functional barriers *in vitro*.

Barrier function *in vitro* is commonly assessed through measurements of molecular and ionic permeability. Molecular permeability is typically quantified using tracer-based assays involving fluorescently labeled solutes or macromolecules[46], whereas ionic permeability is most widely evaluated using trans-endo/epithelial electrical resistance (TEER)[47]. TEER provides a label-free, quantitative metric for tight junction integrity and paracellular ion transport and has therefore become a benchmark technique for assessing barrier formation and disruption in both static culture systems and MPSs.

From a measurement standpoint, TEER can be implemented using either two-point or four-point electrode configurations. In two-point measurements, the same electrode pair is used for both current injection and voltage sensing, resulting in measured

Just Accepted

resistance values that include contributions from electrode–electrolyte interfaces and solution resistance in addition to the barrier itself[48]. While this configuration benefits from structural simplicity and ease of integration, it is inherently sensitive to electrode polarization and contact artifacts. In contrast, four-point measurements decouple current injections from voltage sensing, thereby minimizing interfacial effects and enabling more accurate and reproducible estimation of barrier resistance, particularly under microscale and high-impedance conditions characteristic of MPS environments.

Accordingly, various TEER measurement strategies have been developed for MPS applications, differing primarily in electrode configuration and device integration[48, 49]. Early approaches frequently employed a two-point configuration in which a pair of metal wires was positioned on opposite sides of the cell barrier (**Fig. 2(a)**)[50]. For example, a blood–brain barrier-on-a-chip platform embedded platinum (Pt) wire electrodes in a chip to monitor barrier integrity under shear stress and biochemical modulation[51]. TEER values obtained from this system were comparable to those measured using conventional Transwell™ assays, demonstrating the feasibility of two-wire impedance measurements for barrier assessment in confined microfluidic environments.

To improve measurement accuracy, four-point configurations have been increasingly adopted (**Fig. 2(b)**)[27, 29, 52, 53]. In one representative design, four embedded wire electrodes enabled tetrapolar resistance measurements across cell monolayers, thereby improving measurement robustness and reducing polarization artifacts (**Fig. 2(c)**)[29]. However, reliance on manually inserted wires can complicate device standardization, alignment precision, and scalability, motivating the development of microfabricated electrode configurations and integration strategies.

Fully microfabricated TEER platforms integrate patterned thin-film electrodes directly into the device architecture, typically positioning electrodes above and below the cell layer (**Fig. 2(d)**)[54, 55]. This strategy enables precise control over electrode geometry, spacing, and alignment, thereby confining current paths more effectively across the barrier and improving measurement reproducibility[56]. Subsequent studies have extended this concept by introducing electrode array configurations, allowing spatially resolved TEER measurements and detection of localized barrier disruption and microenvironmental disturbances such as microbubble formation[57, 58].

Moreover, planar TEER configurations, where all electrodes are patterned on a single substrate, have been reported as a fabrication-friendly alternative[55, 59-63]. While such designs simplify fabrication and assembly, careful consideration of current flow geometry is required to ensure that the applied electric field interrogates the barrier in a physiologically relevant manner. Based on this planar electrode structure, four-terminal, thin-film TEER sensing has recently been extended toward spatially resolved barrier monitoring through electrode array integration. In a gut-on-a-chip platform, multiple flexible thin-film electrodes were patterned above and below the epithelial barrier, forming longitudinally distributed tetrapolar sensing units along the culture channel (**Fig. 2(e)**)[64]. Each electrode set functioned as an independent TEER sensing unit, enabling sequential readout of spatially separated regions via multiplexed readout. To improve quantitative accuracy, computational modeling was employed to characterize the electric field distribution and effective sensing area of each unit. This analysis enabled the derivation of geometry-specific correction factors that account for barrier-dependent changes. Collectively, these array-based approaches represent an important step toward resolving spatial heterogeneity in barrier integrity within MPS. Furthermore, more accurate characterization of barrier properties will require spatially resolved and continuous monitoring approaches that account for both barrier heterogeneity and electrode current-path geometry. These requirements should therefore be considered when selecting electrode configurations and integration strategies for TEER-based MPSs.

Just Accepted

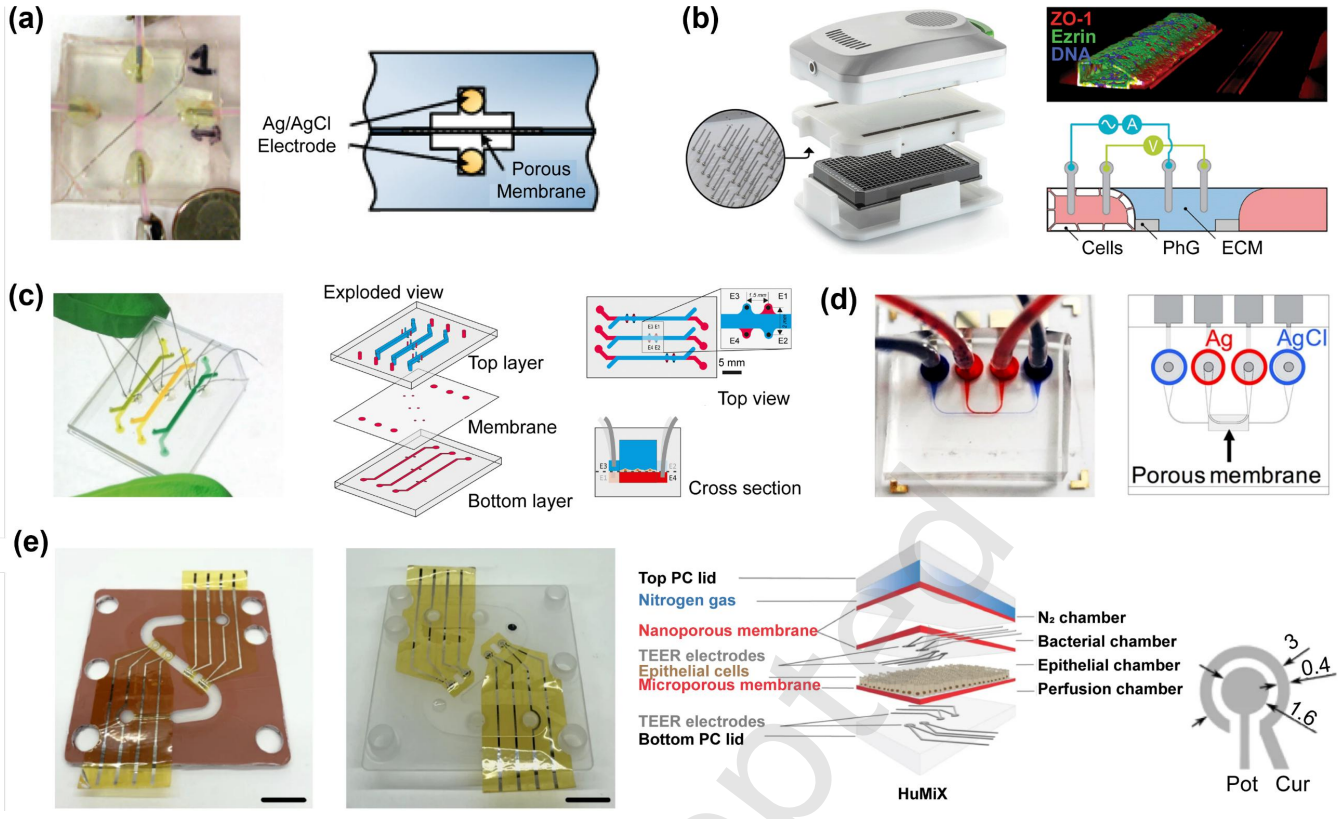


Figure 2 TEER electrode configurations and integration strategies in MPSs.

(a) Two-point electrode configuration for TEER measurement. Reproduced with permission from Ref. [50], © American Chemical Society 2010. (b) MPS incorporating four distinct electrodes, and a schematic representation of the measurement setup and tissue compartments. Reproduced with permission from Ref. [52], © Royal Society of Chemistry 2021. (c) Four-point electrode configuration directly implemented in an MPS. Reproduced with permission from Ref. [29], © Royal Society of Chemistry 2021. (d) Fully microfabricated TEER electrode configuration integrated within a microfluidic device. Reproduced with permission from Ref. [55], © Springer Nature 2017. (e) Vertically aligned four-point electrode configuration employing thin, patterned electrodes integrated above and below a tissue barrier. Reproduced with permission from Ref. [64], © Springer Nature 2024.; TEER: transendothelial/epithelial electrical resistance; PhG: phaseguide; ECM: extracellular matrix; PC: polycarbonate.

2.2 Mechanical responses

Cells and tissues *in vivo* are continuously exposed to diverse mechanical stimuli, including, compression[65], tension[66, 67], and cyclic stretch[68, 69]. These mechanical cues play a central role in regulating a wide range of biological processes, including cell morphology[65, 66, 70], migration[65, 67], differentiation[65], and barrier function[68]. Thus, many MPSs have been designed to reproduce physiologically relevant microenvironments through controlled application of mechanical stimuli. To evaluate how cells and tissues respond to these biomechanical cues, quantitative monitoring of mechanical and mechanobiological responses has become an important component of MPSs.

Mechanical sensing in MPSs enables real-time quantification of cell- and tissue-level properties such as stiffness[70], deformation[71], and contractile force[72]. At the single-cell level, microfluidic platforms have been developed in which geometric confinement within microchannels functions as a mechanical actuator, inducing controlled cell deformation that is transduced into electrical signals via integrated electrodes (**Fig. 3(a)**)[73]. In such systems, cells are perfused through channels with stepwise variations in diameter, where the channel geometry itself functions as a mechanical actuator. As cells traverse constricted regions and subsequently re-enter wider channel segments, they undergo compressive deformation followed by elastic recovery. These deformation–recovery dynamics are directly detected as variations in electrical current using multi-electrode sensors integrated into the microfluidic channel. From these signals, multidimensional mechanical metrics, including deformability, elastic recovery time, and resistance to compression can be extracted, enabling discrimination of mechanical phenotypes associated with cell type, disease state, or malignant progression.

At the tissue level, several MPSs integrated mechanical actuators with embedded sensing elements to probe collective biomechanical behavior. One example is a lung-on-a-chip platform that applied pneumatic actuation to induce cyclic stretching of a compliant alveolar membrane, thereby recapitulating breathing-like motion[72]. Mechanical sensing was achieved using impedance-based electrodes positioned beneath the membrane, allowing non-contact electrical detection of membrane deformation. Changes in deformation amplitude can reflect alterations in the effective stiffness of the membrane–cell composite, enabling indirect quantification of tissue growth and mechanical remodeling without reliance on optical

Just Accepted

deformation tracking[72, 74]. Other platforms have been designed to directly measure tissue-generated forces. For example, heart-on-a-chip platforms incorporating flexible structures and resistive transducers enabled direct electrical readout of contractile forces generated by cardiac microtissues, under externally applied mechanical loading[75]. Such systems provide simultaneous access to mechanical stimulation, intrinsic tissue mechanics, and functional readouts such as beating frequency.

In addition to direct sensing of mechanical force, other sensing approaches have been employed to capture mechanically induced biochemical responses. For example, flexible electrochemical sensors integrated into microfluidic chips enabled real-time monitoring of stretch-induced biochemical signaling from mechanically deformed cells[76]. Together, these sensing approaches expand the capability of MPS platforms to monitor biomechanical responses across multiple spatial and functional scales. Because mechanical responses can change rapidly during cyclic stimulation, contraction, or tissue remodeling, temporally resolved and continuous monitoring is important for capturing their dynamic behavior. These temporal characteristics should therefore guide the selection and integration of mechanical sensing strategies in MPSs.

2.3 Physical microenvironmental parameters

While mechanical sensing focuses on cellular and tissue responses to mechanical stimuli, monitoring the physical microenvironment provides information about the conditions to which these cells and tissues are exposed. In MPSs, key physical microenvironmental parameters include flow rate, shear stress, and hydrostatic pressure, which influence cellular behavior and tissue-level responses[77-79]. Therefore, appropriate control and monitoring of these physical microenvironmental parameters are important for verifying and maintaining physiologically relevant culture conditions in MPSs[80].

Sensing systems for monitoring physical microenvironments in MPSs are designed to convert flow or pressure induced mechanical deformation or changes in electrical properties into measurable signals[81-83]. Flow rate can be quantified based on structural deformation or changes in electrical signals associated with fluid movement[82, 84], whereas hydrostatic pressure can be measured through pressure induced membrane deformation or changes in resistance and capacitance[81, 85]. In contrast, shear stress is often not measured directly but rather derived from the measured flow rate or pressure gradient in combination with channel geometry and fluid viscosity[86, 87]. Accordingly, these sensing approaches enable quantitative assessment of the fluidic microenvironment to which cells are exposed within MPSs.

More recently, various in situ and in-line sensing strategies have been developed to directly monitor physical microenvironments in MPSs and related microfluidic platforms. For example, in a kidney-on-a-chip platform, a miniaturized piezoelectric pressure sensor was integrated near the cell culture region to monitor local hydrostatic pressure within the glomerular microenvironment[88]. In another approach, fiber Bragg grating sensors were embedded within PDMS microchannels to convert flow-induced pressure changes into optical signals, enabling the quantification of both pressure and flow rate based on the pressure–flow relationship[89]. Beyond passive monitoring, physical microenvironment sensing has also been extended toward feedback-controlled regulation, where measured flow or pressure signals are used to maintain stable perfusion conditions[90, 91].

2.4 Metabolic microenvironment and biochemical indicators

Cellular metabolism continuously reshapes the physicochemical microenvironment through the consumption of nutrients and oxygen and the production of metabolic products such as lactate, carbon dioxide (CO_2), and protons. Beyond these metabolic products, cells also modify their biochemical microenvironment through the secretion of signaling molecules, including cytokines, hormones, neurotransmitters, and inflammatory mediators[14]. Accordingly, reproducing such metabolic and biochemical environments in MPSs requires precise control of the culture conditions and quantitative monitoring of the these dynamic molecular states over time[92-94].

Among various metabolic indicators, pH, oxygen, glucose, and lactate are commonly monitored in MPSs because they collectively capture substrate availability, metabolic flux, and waste accumulation. pH serves as an integrative indicator of glycolysis, CO_2 production, and lactate accumulation[95-97], while oxygen availability directly governs mitochondrial respiration and metabolic strategy[98, 99]. Glucose and lactate measurements provide complementary information on nutrient consumption and glycolytic flux[100], enabling assessment of perfusion efficiency and metabolic reprogramming, and tissue-specific metabolic phenotypes[101-105].

Early *in vitro* studies typically assessed metabolic status through offline analysis of bulk culture medium (**Fig. 3(b)**)[106], or by collecting perfusate samples for biochemical assays[107]. While such approaches provided useful averaged information, they were limited in temporal resolution and lacked the ability to resolve local microenvironmental dynamics. As MPS technologies matured, metabolic sensing strategies progressively shifted toward on-chip and *in situ* monitoring, allowing continuous quantification of metabolite production and consumption and facilitating broader monitoring of dynamic biochemical changes under dynamic flow conditions[43].

Optical sensing strategies, particularly those based on photoluminescent reporters, have been widely adopted for non-invasive monitoring of oxygen and pH in MPSs[16, 108-116]. By dropwise deposition of oxygen-responsive microparticles from solution within microfluidic culture chambers or channel walls, these microparticles function as localized oxygen sensors, enabling spatially resolved measurements of oxygen gradients without introducing electrical interfaces into the biological

Not Accepted

compartments (**Fig. 3(c)**)[117]. Such approaches are especially advantageous for three-dimensional (3D) tissues, where optical access allows interrogation of metabolic heterogeneity across depth and time.

In parallel, electrochemical sensing strategies have been extensively integrated into MPS to quantify metabolites such as glucose and lactate, whose detection relies on enzymatic redox reactions or ion activity (**Fig. 3(d)**)[16, 115, 118-121]. Amperometry sensors patterned as thin-film microelectrodes enabled real-time, label-free monitoring within confined microfluidic channels. In another study, multi-analyte sensor arrays for oxygen, glucose, and lactate measurements have demonstrated the ability to capture coordinated metabolic shifts, including hypoxia-induced glycolytic activation in cancer stem cell cultured within a 3D ECM (**Fig. 3(e)**)[122]. In addition to metabolic monitoring, a BBB-on-a-chip integrated with immunosensors enabled multiplexed and longitudinal monitoring of cytokine secretion from brain endothelial barriers, revealing polarized secretion profiles that could not be readily captured by conventional endpoint assays[123]. Together, these examples highlight the potential of integrated sensing approaches to characterize metabolic activity as well as biochemical signaling within MPSs.

2.5 Electrophysiological activity

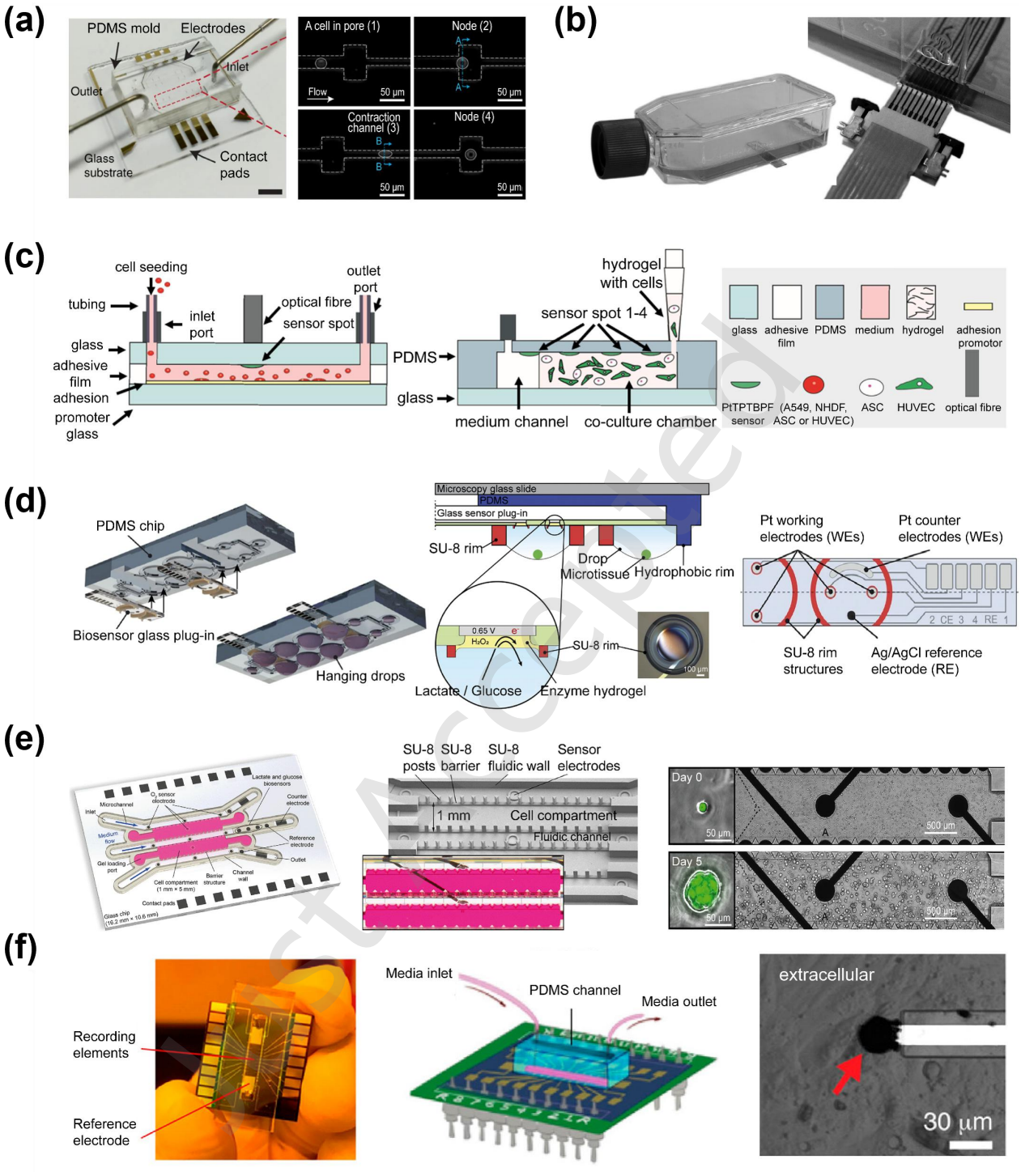
Electrically excitable tissues, including the nervous system and cardiac tissues, generate and propagate action potentials to perform their physiological functions[124]. These electrical signals govern essential biological processes such as neuronal communications, rhythmic contraction, and tissue-level synchronization. Electrophysiological monitoring is therefore a critical tool for evaluating tissue viability, functional maturation, intercellular coupling, and responses to pharmacological or pathological stimuli in MPSs that recapitulate electrically active tissues, including cardiac[125], neural[126], and pancreatic islet systems[127].

Microelectrode arrays (MEAs) are widely used for long-term electrophysiological monitoring in MPSs[128], owing to their ability to record spatially distributed signals with high temporal resolution while remaining compatible with long-term culture. Thin-film MEAs integrated into microfluidic platforms have enabled simultaneous measurement of electrophysiological parameters, such as firing or beating frequency[129], and network synchronization[130]. Their planar geometry facilitated precise alignment with cell layers and preserved optical accessibility for complementary imaging.

In cardiac MPSs, for example, MEA integration allowed continuous recording of spontaneous extracellular field potentials generated by engineered cardiac tissues, providing quantitative assessment of tissue electrophysiology under different conditions (**Fig. 3(f)**)[125]. Similarly, in a neuronal MPS, MEA integration enabled direct recording of axonal electrophysiological activity, allowing propagation of individual action potentials to be resolved along isolated axons[126]. Collectively, these studies demonstrate that MEA-integrated MPSs provide stable, long-term, and spatially resolved functional evaluation of electrically active engineered tissues.

Just Accepted

Figure 3 Representative sensor-integrated MPSs for monitoring physiological functions and microenvironments. (a) Microfluidic platform incorporating integrated mechanical actuator and electrodes for quantifying cell-level mechanical



properties. Reproduced with permission from Ref. [73], © Springer Nature 2018. (b) Sensor-based approach for monitoring pericellular oxygen levels in conventional flask cultures. Reproduced with permission from Ref. [106], © John Wiley & Sons Ltd 2014. (c) Non-invasive optical oxygen sensing approach for real-time monitoring in two- and three-dimensional microfluidic culture models. Reproduced with permission from Ref. [117], © Frontiers Media S.A 2018. (d) Microfluidic platform integrating enzyme-based multi-analyte biosensor interface. Reproduced with permission from Ref. [121], © Springer Nature 2016. (e) MPS incorporating integrated electrochemical microsensors for multi-analyte metabolic monitoring. Reproduced with permission from Ref. [122], © Royal Society of Chemistry 2022. (f) MPS integrating extra- and intracellular electrodes for monitoring cardiac electrophysiological activity under hypoxic conditions. Reproduced with permission from Ref. [124], © American Chemical Society 2020.; PDMS: polydimethylsiloxane; PMMA: polymethyl methacrylate.

3 Fabrication strategies for sensor integration in MPS

3.1 Bottom-up fabrication approaches for sensor integrated MPS

Accepted

Bottom-up approaches for sensor integration in MPSs can be broadly categorized into MEMS-based microfabrication and additive and printed fabrication approaches. These two approaches differ fundamentally in achievable resolution, process flexibility, material compatibility, and scalability, thereby serving complementary roles in the development of sensor-integrated MPSs.

MEMS-based fabrication offers high-resolution, reproducible patterning of microscale electrodes and circuits[131, 132], making it a major strategy for integrating microscale electrodes and circuits into MPSs. Alternative approaches, including additive and printed fabrication method utilizing solution-based patterning, allow rapid prototyping, low-temperature processing, and compatibility with soft or 3D substrates. These approaches complement MEMS fabrication by addressing practical limitations associated with cleanroom access, iterative design cycles, and compatibility with complex or heterogeneous MPS geometries. In the following sections, we review these two fabrication strategies and discuss how their intrinsic process characteristics translate into sensor performance, integration feasibility, and long-term reliability in MPS environments.

3.1.1 MEMS-based fabrication

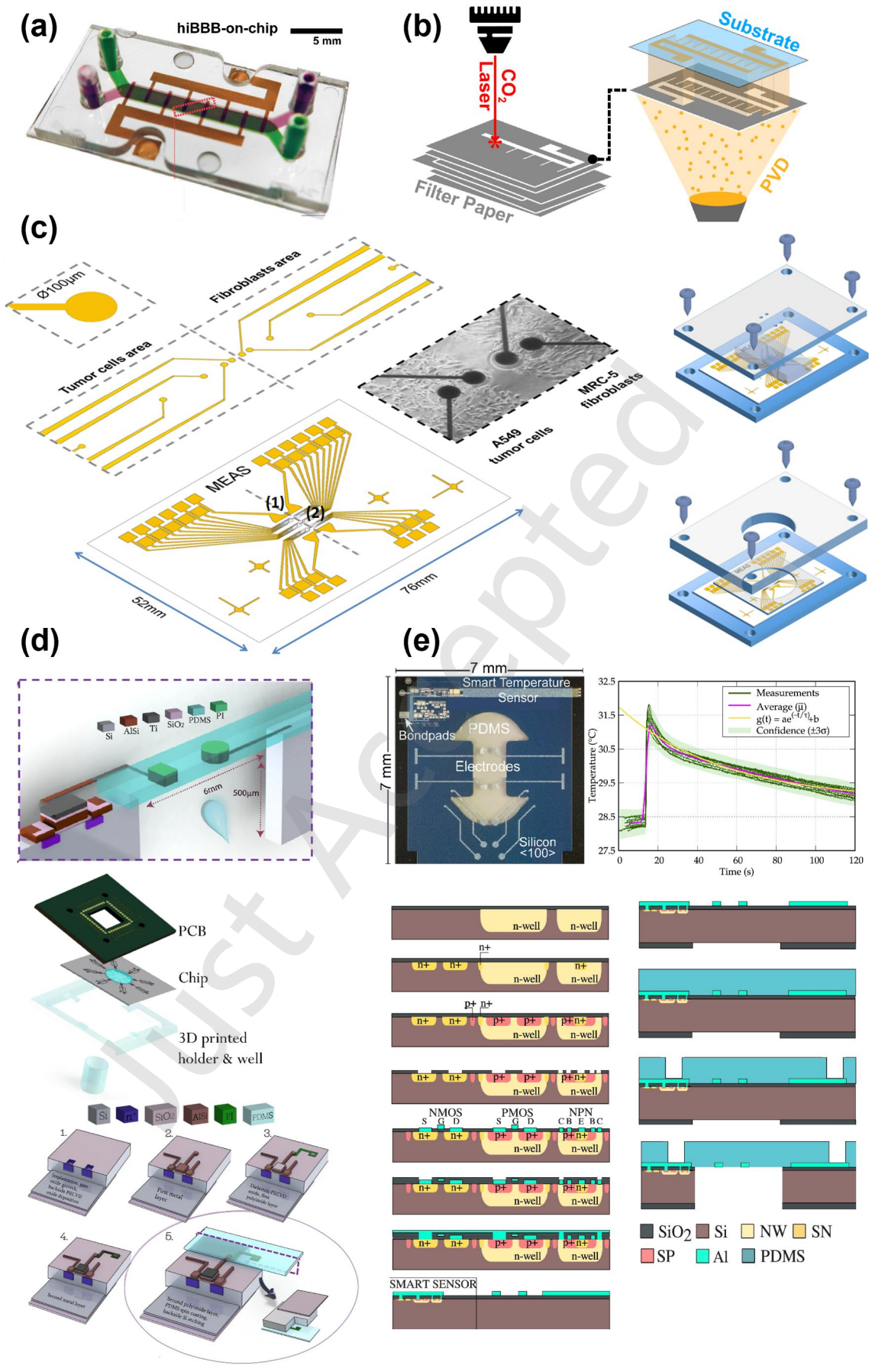
MEMS technology enables the fabrication of microscale structures and systems with integrated electronic or electromechanical components[133]. Originating from semiconductor integrated circuit (IC) manufacturing[134, 135], MEMS technologies have since expanded to support the fabrication of 3D microstructures[136-138], electronic circuits[139-141], sensors[142-144], and actuators[145-147] across a wide range of applications.

For MPS applications, MEMS-based fabrication is particularly attractive because sensor elements can be miniaturized, precisely patterned, and robustly integrated within confined microscale environments[148, 149]. Moreover, MEMS fabrication provides high reproducibility and compatibility with scalable manufacturing workflows, making it well suited for the scalable and reproducible production of sensor-integrated MPSs. Importantly, MEMS processes enable accurate alignment of sensing elements relative to biological components, which is critical for sensing modalities including TEER measurement, impedance spectroscopy, and electrophysiological recording. In addition, MEMS-based sensors can be incorporated into a unified device process flow, allowing either pre-fabrication of sensors on a substrate prior to microfluidic assembly or post-processing integration depending on material compatibility and bonding constraints.

MEMS-based fabrication has enabled integration of a wide range of sensor architectures into MPSs (**Table 2**). Thin-film metal electrodes patterned via sputtering[54, 150-152] or electron-beam evaporation (**Figs. 4(a)~(c)**)[56, 59, 75, 153-160] are commonly employed for TEER measurements, electrochemical biosensing, and impedance-based monitoring. Such electrodes provide well-defined geometry, stable electrical performance, and compatibility with biochemical surface functionalization, making them suitable for long-term *in situ* sensing under continuous perfusion[56].

Beyond single-electrode configurations, MEMS processes also enable the fabrication of multiplexed electrode arrays and circuit-level integration, allowing spatially resolved sensing and parallel signal acquisition (**Fig. 4(d)**)[161]. In more advanced implementations, complementary metal-oxide semiconductor (CMOS)–MEMS co-fabrication strategies have been employed to integrate active electronic components, such as transistor-based temperature or impedance sensors, directly into MPSs (**Fig. 4(e)**)[162]. Collectively, these studies highlight the versatility of MEMS technology for fabrication of passive sensing interfaces and active electronic functionalities, thereby supporting increasingly sensitive and multifunctional sensor-integrated MPSs.

Just Accepted



Just Accepted

Figure 4 MEMS-based sensor fabrication and integration in MPSs.
(a) Fabrication of planar thin-film electrodes using electron-beam evaporation. Reproduced with permission from Ref. [59], © Wiley-VCH 2021. (b) Fabrication schematic corresponding to the electrodes shown in (a), using a laser-cut paper shadow mask for PVD. Reproduced with permission from Ref. [153], © MDPI 2020. (c) Microelectrode arrays fabricated through common photolithography processes. Reproduced with permission from Ref. [158], © PLOS 2016. (d) Integration of microsensors into

MPS through CMOS–MEMS co-fabrication, allowing for on-chip circuitry and robust sensor operation. Reproduced with permission from Ref. [161], © Springer Nature 2023. (e) Sensor fabrication based on photolithography with integrated dielectric layers, facilitating electrical isolation and multilayer device architectures. Reproduced with permission from Ref. [162], © Elsevier 2021.; hiBBB: human induced pluripotent stem cell-derived blood-brain barrier; PVD: physical vapor deposition; PI: polyimide; PDMS: polydimethylsiloxane; PECVD: plasma-enhanced chemical vapor deposition; NW: n-well; SN: n-type diffusion; SP: p-type diffusion.

3.1.2 Additive and printed fabrication approaches

While MEMS-based fabrication remains a dominant strategy for sensor integration, additive and printed fabrication approaches have emerged as complementary technologies that offer greater design flexibility and fabrication accessibility. Compared with MEMS-based fabrication, additive approaches require less specialized infrastructure and enable rapid design iteration, making them particularly attractive for customized MPS architectures and prototyping.

Additive and printed electronics have attracted considerable interest in sensor integration into MPSs, as they enable digitally programmable and often mask-free patterning of conductive and functional materials at low temperatures[163]. As a result, electrodes and sensing elements can be directly deposited onto diverse substrates, including polydimethylsiloxane (PDMS), polyimide (PI), polyethylene terephthalate (PET)[58], polymethyl methacrylate (PMMA)[164], and glass[165] using functional materials ranging from metal- or carbon-based inks to conductive polymer, nanocomposites, hydrogels, and liquid metals. Representative examples include metals such as Au, Ag, Ag/AgCl, and Pt[58, 163-166], conductive polymers such as PEDOT: PSS, conductive carbon[58, 167, 168], and even liquid metals[169, 170]. This capability is particularly attractive for MPS devices that incorporate curved surfaces, multilayer architectures, or soft elastomeric materials, where conventional planar microfabrication approaches may be difficult to implement (**Table 3**).

Inkjet printing and screen printing have been widely employed to fabricate electrochemical sensors (**Fig. 5(a)**)[171], TEER electrodes (**Fig. 5(b)**)[58], and impedance-based sensing elements (**Fig. 5(c)**)[172] within microfluidic systems. Inkjet printing offers precise spatial patterning and efficient material usage through drop-on-demand deposition of picoliter-scale droplets [173]. These characteristics make inkjet printing attractive for localized fabrication of sensing elements within microfluidic systems and MPSs. Screen printing, in contrast, uses high-viscosity conductive pastes and patterned masks to produce mechanically robust electrodes over larger areas with minimal equipment requirements[174-177]. Other deposition techniques such as spray printing have also been explored primarily for large-area or conformal coatings, although their application to spatially resolved sensing within MPSs remains limited[166, 178].

More recently, 3D printing has been increasingly explored for the fabrication and integration of sensing elements within MPSs. Compared with conventional inkjet or screen printing, 3D printing not only enables the fabrication of complex 3D structures but also allows different functional materials to be integrated within a single programmable fabrication process[167, 168]. In particular, direct ink writing (DIW) enables direct patterning of functional inks at desired locations within MPSs without requiring photolithographic masks, making it particularly attractive for sensor-integrated MPSs that require both complex architectures and diverse functional materials. For example, a multimaterial DIW approach has been reported in which six functional materials were sequentially patterned within a single fabrication workflow[167]. These materials were integrated to form piezoresistive strain sensors, electrical interconnects, and tissue-guiding structures, enabling the fabrication of a cardiac MPS capable of continuous monitoring of cardiac contractile stress.

The high material versatility of such direct-write fabrication approaches further extends the range of conductive materials beyond conventional solid metals to soft conductive materials such as liquid metals. Owing to their high electrical conductivity, deformability, and lower mechanical stiffness compared with conventional rigid metals, liquid metals have been increasingly explored for 3D biological interfaces. In one example, eutectic gallium–indium (EGaIn) was directly printed through a nozzle to fabricate height-adjustable 3D microelectrode arrays, which were subsequently applied to record spatially resolved electrophysiological signals within brain organoids[170].

While additive fabrication approaches have provided substantial advantages in terms of fabrication flexibility, cost reduction, and substrate compatibility, they generally offer lower pattern resolution and higher variability compared to MEMS processes. Electrode performance may be affected by ink formulation, sintering conditions, surface roughness, and long-term material stability. Taken together, additive fabrication is often employed either in combination with MEMS-fabricated structures or in applications where rapid prototyping, disposability, and design flexibility outweigh the need for microscale precision.

Just Accepted

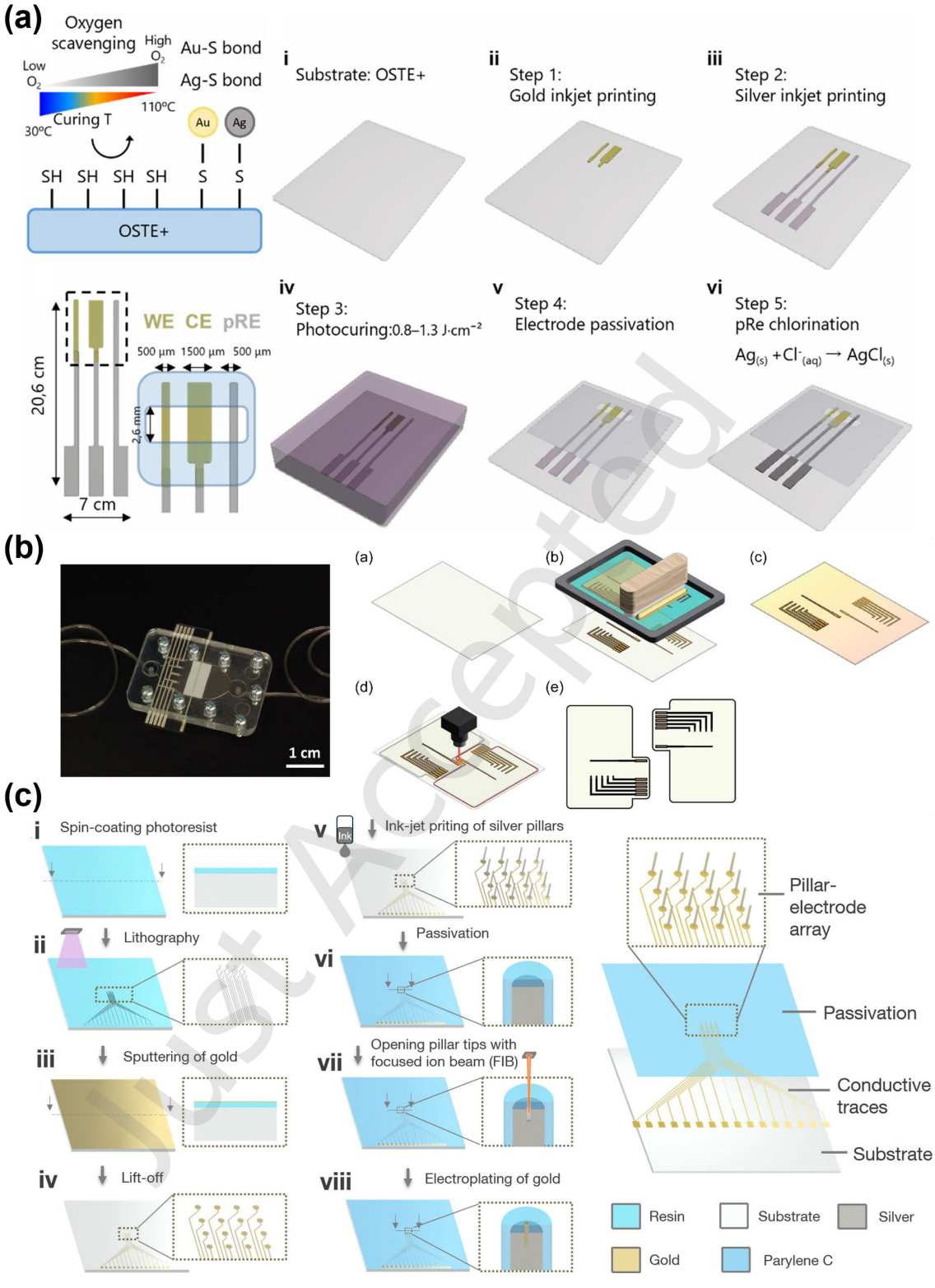


Figure 5 Representative additive and printed-based fabrication approaches for sensor integration in MPSs. (a) Inkjet-printed electrochemical oxygen sensor fabricated through low-temperature, mask-free deposition and photocuring. Reproduced with permission from Ref. [171], © Royal Society of Chemistry 2026. (b) Screen-printed electrode platform highlighting rapid and scalable fabrication of integrated sensor elements. Reproduced with permission from Ref. [58], © American Chemical Society 2023. (c) Hybrid fabrication strategy combining high-aspect ratio pillar electrode arrays with tunable geometries. Reproduced with permission from Ref. [172], © American Chemical Society 2025.

3.2 Top-down fabrication approaches for sensor-integrated MPS

In contrast to bottom-up approaches that fabricate sensing elements directly within MPSs, top-down strategies integrate pre-

Just Accepted

fabricated, commercially available sensors into MPSs. This approach prioritizes measurement robustness, calibration reliability, and system-level reproducibility over miniaturization or geometric flexibility.

One major advantage of top-down integration is the use of pre-calibrated sensing elements, which significantly reduces device-to-device variability and long-term signal drift in extended MPS culture. Optical sensing modules for pH and oxygen are among the most widely adopted examples[179]. These systems typically employ commercially available light-emitting diodes (LEDs), photodiodes, and luminescent or absorbance-based indicators mounted externally or in dedicated detection chambers connected to the perfusion loop. Because the sensing components are often physically separated from the biological chamber, optical access is preserved while minimizing perturbation to the cellular microenvironment.

Electrochemical probes and electrode assemblies have also been incorporated through top-down strategies, particularly for monitoring metabolic indicators such as glucose, lactate, and oxygen[180]. In such configurations, electrodes are often positioned at the inlet or outlet regions of the microfluidic circuit, allowing continuous monitoring of bulk medium composition without interfering with local tissue architecture. These configurations provide stable and repeatable measurements, making them well suited for long-term perfusion experiments.

Commercial sensors originally developed for clinical applications have also been adapted for use in MPS platforms. For example, a commercially available continuous glucose monitor, FreeStyle Libre, was adapted for use in a tumor-on-chip platform to continuously measure glucose concentrations for approximately two weeks, enabling the evaluation of cellular glucose consumption and drug-induced metabolic changes[104].

Despite their advantages for sensor-integrated MPS fabrication, top-down approaches have inherent limitations, including restricted spatial resolution, reduced flexibility in sensor placement, and challenges in integrating multiple sensing modalities within compact device footprints. Commercially available sensors may require additional fluidic interfacing for compatibility with MPS platforms[91]. Moreover, sensor placement should be carefully considered, as measurements obtained from external perfusion circuits may reflect bulk medium conditions rather than localized changes within the cellular microenvironment[55]. Thus, top-down strategies are often used together with bottom-up fabrication methods, resulting in hybrid systems that balance robustness with spatial specificity.

3.3 Comparative assessment of fabrication and integration strategies

Overall, MEMS-based fabrication, additive/printed fabrication, and top-down integration of commercial sensors offer distinct trade-offs in fabrication complexity, scalability, cost, reproducibility, and biocompatibility. MEMS-based approaches provide high patterning resolution and reproducibility but generally require specialized infrastructure and complex fabrication processes that increase fabrication complexity and cost. In contrast, additive and printed fabrication enables rapid prototyping, lower infrastructure requirements, and greater compatibility with diverse substrates, offering advantages for scalable fabrication, although resolution and device-to-device reproducibility can be more dependent on processing conditions. The integration of commercially available sensors can reduce the need for custom sensor fabrication and facilitate reproducible measurements, but may limit flexibility in sensor placement and miniaturization and require additional interfacing with MPS platforms. Biocompatibility should also be considered for all three approaches, particularly with respect to substrate properties, residual processing materials, and the compatibility of sensor materials with long-term cell culture.

4 Design considerations and precautions for sensor-integrated MPS

Although diverse sensing modalities and fabrication strategies have enabled real-time monitoring of physiological signals in MPSs, successful sensor integration requires considerations beyond sensing performance alone. Unlike conventional *in vitro* assays, MPSs operate within confined volumes, under continuous perfusion, and over extended culture durations, where sensor placement, material selection, and signal transduction can directly perturb the biological system. Despite recent advances, several cross-cutting bottlenecks remain, including accurate measurement of spatially and temporally heterogeneous signals, minimally perturbative sensor–tissue integration, maintenance of sensor stability and calibration during long-term culture, and reproducible integration of multiple sensing components within scalable MPS platforms. Therefore, sensor design must balance measurement accuracy with preservation of tissue function, long-term stability, and practical manufacturability.

Sensor selection and integration in MPS should be guided by the physiological target and its measurement requirements, rather than fabrication convenience alone[29, 52]. These requirements affect the choice of sensing principles, fabrication methods, and sensor placement. For example, electrode-based sensing is appropriate for monitoring electrical activity, whereas electrochemical and affinity-based approaches can be used to detect specific metabolites and biomarkers[181, 182]. In addition, biochemical targets, such as cytokines and metabolites, often require sensitive and selective electrochemical and affinity-based sensing[181, 182]. MEMS-based fabrication can provide precise electrode alignment and spatial control[161, 162], while printing-based fabrication can accommodate complex 3D geometries or soft tissue interfaces[58, 163]. Importantly, sensor placement should account for analyte transport, diffusion distance, and tissue architecture. Accordingly, sensing principles, fabrication methods, and integration geometries should be selected in a coordinated manner based on the target physiological signal and required measurement performance.

In practice, sensor selection involves trade-offs among spatial and temporal resolution, sensitivity, response time, and detection throughput. The relative importance of these parameters depends on the physiological signal and the intended measurement. For example, rapidly varying electrophysiological signals require high temporal resolution and faster sensor

Just Accepted

response[183, 184], whereas low-abundance biomarkers require careful consideration on sensitivity and selectivity[123, 153]. Spatial resolution is particularly important for resolving heterogeneous responses within tissues, while detection throughput may be emphasized when monitoring multiple analytes or comparing numerous MPS conditions. Therefore, sensor performance should be optimized according to the specific biological question rather than maximizing individual performance metrics independently. This section discusses key design considerations for sensor-integrated MPSs, focusing on sensor placement, electrochemical stability, biocompatibility, long-term reliability, economic feasibility, and emerging data-assisted strategies.

4.1 Sensor placement and spatial configuration

Sensor performance in MPSs is strongly affected by spatial placement, as both signal detectability and measurement accuracy depend on the transport dynamics and lifetime of the target analyte. For short-lived species such as dissolved oxygen[34] or reactive oxygen species (ROS)[185], sensors should be positioned in close proximity to the cells to capture steep spatial gradients that dissipate rapidly with distance. For instance, optical oxygen sensors positioned directly beneath 3D induced pluripotent stem cell (iPSC)-derived human cardiac spheroids enabled quantification of local oxygen partial pressure (pO_2) within the 3D tissue construct, which would not be detectable using outlet-based measurements[186]. In contrast, more stable metabolites, such as glucose and lactate, can often be monitored downstream, allowing sensor placement that minimizes perturbation to the tissue microenvironment while still providing representative information on metabolic activity[122].

Certain sensing modalities impose additional geometric constraints. In TEER measurements, electrodes should be aligned such that the applied electric field traverses the epithelial or endothelial barrier perpendicularly, ensuring a uniform current distribution across the cell layer (**Fig. 6(a)**)[47, 57, 152, 187]. Improper electrode alignment can distort the electric field distribution, leading to measurement artifacts that may compromise accurate quantification of barrier properties. Collectively, these examples highlight that sensor placement should be guided not only by fabrication convenience but also by analyte transport physics, sensing modality, and the spatial organization of the engineered tissue.

4.2 Electrochemical considerations

Electrochemical sensing is one of the most widely adopted monitoring strategies in MPSs because it enables continuous, label-free measurement of barrier function, metabolic activity, and electrophysiological signals. However, the performance of electrochemical sensors is fundamentally governed by processes occurring at the electrode–electrolyte interface, which directly affect signal accuracy, stability, and long-term reliability. These considerations become especially important in MPSs, where sensors operate in confined volumes with protein-rich media under continuous perfusion.

The choice of electrode material is a primary determinant of interfacial electrochemical behavior. Noble metals such as gold (Au) and Pt are widely used because of their excellent electrical conductivity, chemical stability, biocompatibility, and compatibility with microfabrication processes. These properties make them suitable for long-term operation in biological environment. However, even highly stable electrode materials are susceptible to electrode polarization, in which charge accumulation at the electrode-electrolyte interface introduces additional impedance and distorts measured signals, particularly in impedance- and resistance-based measurements.

To minimize polarization-induced artifacts, multi-electrode configurations are frequently employed. Among these, the four-point electrode configuration is widely adopted because it separates current injection from voltage-sensing, reducing the influence of electrode–electrolyte interfacial impedance on the measured signals[188]. In TEER-integrated MPSs, four-point configurations have been shown to improve both measurement accuracy and reproducibility compared with conventional two-point configurations, particularly during long-term monitoring[64].

Beyond electrode geometry, surface engineering represents an additional strategy for reducing polarization and improving electrochemical performance. Surface coatings based on highly electrochemically active materials, such as Pt black, iridium oxide[188], and conductive polymers (e.g., poly(3,4-ethylenedioxythiophene) polystyrene sulfonate (PEDOT:PSS)[189]), have been widely used to increase the effective electrode surface area and reduce interfacial impedance[155]. These modifications improve signal sensitivity and signal-to-noise ratio while allowing more stable measurements. However, their mechanical durability and electrochemical stability under continuous perfusion and biological exposure should be carefully evaluated for long-term applications.

For target-specific electrochemical biosensing, the sensing interface requires a recognition element tailored to the analyte. Ions are commonly detected using ion-selective membranes containing ionophores, whereas small-molecule metabolites such as glucose and lactate are typically detected using enzymes. Proteins or cytokines can be detected using affinity-based receptors such as antibodies or aptamers. Here, the analytical performance of electrochemical biosensors depends on both the electrode/transduction system and the selectivity, affinity, and stability of the recognition element[41].

Recognition elements involve distinct trade-offs in selectivity, response time, regeneration, and long-term stability. Ion-selective membranes generally enable rapid and reversible detection, while enzyme-based sensors provide high substrate specificity but may lose activity during prolonged operation. Antibody-based sensors offer high affinity for protein biomarkers but are often limited by surface saturation and poor regeneration, whereas aptamers can provide more reversible affinity recognition in selected configurations. These differences are particularly relevant to MPSs, where continuous perfusion,

Just Accepted

protein- containing culture media, and extended operation can accelerate signal drift, surface saturation, and loss of recognition activity[41, 190].

Another major challenge is biofouling at the sensor interface[190]. Adsorption of proteins, cells, and biomolecules can progressively alter surface chemistry, reduce sensitivity, and induce signal drift. To mitigate these effects, antifouling surface coatings[191] and strategic sensor placement that minimizes direct exposure to cellular regions have been employed. Because biofouling mechanisms vary substantially depending on cell type, culture duration, and medium composition, no single mitigation strategy is universally applicable, highlighting the importance of application-specific sensor design.

Finally, electrochemical sensing itself can perturb the local biological microenvironment through reaction byproducts or localized physicochemical stress. Enzyme-based biosensors generate reactive species such as hydrogen peroxide, while metal electrodes may induce local pH shifts or ion release. In the confined microfluidic environments in MPSs, such effects can become amplified and potentially influence cellular behavior, requiring careful control of current density, reaction kinetics, and perfusion conditions to preserve biological fidelity. Accordingly, the design of electrochemical sensors in MPSs should consider not only electrode material and geometry but also the target analyte, recognition mechanism, measurement duration, and the need for repeated or continuous monitoring.

4.3 Biocompatibility and long-term stability

The successful operation of sensor-integrated MPSs depends not only on sensing performance but also on the ability of sensing components to coexist with living tissues over extended culture periods. Consequently, both biocompatibility and long-term stability must be considered during sensor design and device integration.

Biocompatibility is influenced not only by the intrinsic properties of the sensing materials, but also by the methods used to assemble, bond, and seal the device. Even when sensor substrates are inherently biocompatible, incomplete curing of adhesives or residual solvents can leach into the culture medium and induce cytotoxic effects[50]. Accordingly, a variety of integration strategies have been adopted, including adhesive-free bonding methods (**Fig. 6(b)**)[192], ultraviolet (UV)-adhesives, and polymer-based bonding methods[51]. In many cases, bonding regions are spatially isolated from cell culture compartments to reduce direct exposure of tissues to potentially harmful materials. Such considerations are particularly important for long-term experiments, where even low levels of chemical leaching or degradation may accumulate over time and affect cellular behavior.

Long-term sensor stability in MPSs is often affected by gradual signal drift arising from both biological and material-related factors. Changes in pH, ionic strength, and metabolite composition can alter electrode surface properties and enzyme activity, thereby altering sensor sensitivity and compromising calibration accuracy. At the same time, mechanical stress and continuous perfusion may induce delamination, microcracking, or degradation of thin-film structures and interconnects[34]. Optical sensing platforms are likewise affected by photobleaching and dye degradation during repeated and prolonged illumination[193]. Importantly, long-term signal drift rarely originates from a single failure mode, but rather reflects the cumulative effects of biochemical, mechanical, and photophysical processes. Calibration is another important consideration for extended monitoring, as sensor sensitivity and baseline responses may change during prolonged exposure to culture conditions. Calibration performed before an experiment may therefore not fully represent sensor performance at later time points[34, 194]. Depending on the sensing modality, periodic or in situ recalibration, reference measurements, and pre- and post-experiment calibration can be employed to distinguish true biological changes from sensor-induced signal drift[122, 192, 195]. Accordingly, the appropriate calibration strategy should be selected based on the expected drift behavior and intended monitoring duration.

Therefore, maintaining reliable sensor performance over extended culture requires a combination of biocompatible materials, mechanically robust device architectures, stable sensing and recognition chemistries, effective mitigation of biofouling, and appropriate calibration or recalibration strategies tailored to the intended monitoring duration.

4.4 Economic and manufacturing considerations

Economic considerations play an important role in determining the accessibility, reproducibility, and scalability of sensor-integrated MPSs. While high-performance sensing is often the primary objective, fabrication cost and manufacturing complexity can strongly affect the feasibility of routine implementation and large-scale adoption. Importantly, economic feasibility depends not only on the cost of materials and equipment but also on manufacturing throughput, process scalability, and reproducibility across devices and production batches.

Photolithography-based cleanroom fabrication offers high-resolution patterning and high reproducibility, making it a widely applicable approach for sensor integration. However, the associated costs of specialized facility, equipment, and trained personnel can limit accessibility and scalability[196]. To address these limitations, additive and printing-based fabrication approaches that eliminate mask fabrication and vacuum processing have gained attention as lower-cost, high-throughput alternatives, supported by continuous advances in materials and process control[163, 197].

Material selection further impacts economic viability. Although noble metals provide excellent electrochemical performance and long-term stability, their cost can become restrictive for large-area devices, high-density sensor arrays, or disposable applications. Consequently, cost-effective functional materials including carbon-based materials (e.g., graphene, carbon

Just Accepted

nanotubes, and conductive carbon inks) are increasingly explored as alternatives that balance performance with manufacturability and scalability[164].

Importantly, economic considerations should be aligned with the intended purpose of sensor operation. Disposable sensing platforms designed to minimize cross-contamination and long-term signal drift are well suited to low-cost materials and simplified fabrication workflows. In contrast, applications requiring extended operation and repeated measurements may justify the use of more expensive materials and fabrication processes owing to their superior durability and long-term stability. Collectively, these considerations highlight that economic constraints should not be considered independently from sensor performance. Rather, cost, reliability, manufacturing throughput, reproducibility, scalability, and application requirements must be balanced simultaneously to enable practical and scalable implementation of sensor-integrated MPSs.

4.5 Multimodal sensing and system-level integration

Physiological responses within native tissue microenvironments are not represented by a single signal, but rather arise from coordinated changes in multiple features including barrier integrity, electrophysiological activity, mechanical function, metabolic activity, and the surrounding microenvironment[39, 198]. Accordingly, multimodal sensing capable of simultaneously measuring different types of physiological signals is emerging as an important strategy for more comprehensive functional assessment of MPSs. In particular, continuous measurement of multiple signals along the same temporal axis enables correlation of electrical, mechanical, metabolic, and barrier responses to a given stimulus[115, 199, 200].

Several multimodal MPS platforms have demonstrated the benefits of combining complementary sensing modalities. For example, a heart-on-a-chip platform combining MEA and TEER measurements enabled simultaneous assessment of cardiac electrophysiology and endothelial barrier function[155]. By tracking multiple functional changes in response to external stimuli such as tumor necrosis factor alpha (TNF-α) and isoproterenol, this study demonstrated the value of multimodal sensing. For monitoring coordinated metabolic changes, multi-analyte electrochemical sensor arrays for oxygen, glucose, and lactate have been integrated into MPSs [115]. In another example, a gut/liver-on-a-chip platform combined TEER, oxygen, and pH monitoring with ATP/ADP metabolic reporters and analyses of cellular morphology and phenotype, enabling continuous and non-invasive monitoring for up to 23 days[199].

Despite these advantages, integrating multiple sensing modalities within a single MPS introduces several technical challenges in terms of both physical implementation and data processing. From a hardware perspective, different sensing principles require distinct electrode materials, optical access, surface functionalization, wiring schemes, and readout electronics, thereby increasing overall system complexity and creating spatial constraints within confined microfluidic architectures[39, 40]. Furthermore, the incorporation of multiple sensors and auxiliary components may perturb local fluid flow or tissue morphology and can also introduce electrical, chemical, or optical interference between sensing elements[40, 201].

Moreover, direct comparison and integration of heterogeneous datasets are challenging as each sensing modality typically operates with different sampling rates, dynamic ranges, response times, and calibration requirements. Accordingly, multimodal platforms must address not only the spatial arrangement and fabrication compatibility of sensing elements but also temporal synchronization, data normalization, signal-drift correction, and cross-modal data alignment to distinguish true biological responses from artifacts introduced by sensor integration[201, 202]. Ultimately, next-generation multimodal MPSs will require integrated data acquisition and analysis frameworks that support synchronized measurements and reliable interpretation of heterogeneous data streams[201, 202].

4.6 Emerging AI-assisted design optimization and signal processing

Data-driven approaches are emerging as promising tools for both the design optimization and signal processing of sensor-integrated MPSs. Although AI has not yet been widely applied directly to sensor fabrication or integration within MPSs, studies in related fields such as microfluidics, sensor engineering, and materials science demonstrate its potential as a design-assistive framework. For example, deep-learning models have been applied to microfluidic soft pressure sensors to decode nonlinear and hysteretic sensor responses to infer pressure magnitude and spatial distribution, thereby enhancing sensor performance without altering the physical device architecture[203].

Machine-learning frameworks, including Bayesian optimization and deep learning, have also been used to optimize microchannel geometries (**Fig. 6(c)**)[204] and predict flow profiles[205]. These studies suggest that similar approaches could guide sensor placement to minimize signal interference and perturbation to cellular microenvironments. In parallel, AI-based material prediction models, such as those used to estimate electrochemical sensitivity[206] or detection limits for functional materials[207], highlight the potential for data-assisted selection of electrode materials and surface modifications. By coupling experimental data with computational models, AI-assisted design may enable rational exploration of large and highly multidimensional design spaces that are difficult to navigate through empirical trial-and-error approaches alone. In particular, design variables such as microchannel geometry, electrode dimensions, sensor placement, and material properties can be linked to specific performance objectives, including flow uniformity, sensing sensitivity, spatial resolution, and minimal perturbation of the cellular microenvironment. Such data-driven optimization may help identify suitable design configurations while accounting for trade-offs among these competing requirements. These capabilities are particularly attractive for sensor-integrated MPSs, where fabrication parameters, sensing performance, biological compatibility, and operational stability are

Just Accepted

often interdependent.

Beyond these design-stage applications, data-driven approaches can support nonlinear calibration, noise reduction, drift correction, interference compensation, and automated feature extraction from sensor outputs[202, 208, 209]. For example, regression-based models can be used to calibrate nonlinear sensor responses[210], machine-learning algorithms to correct signal drift[211], and classification models to distinguish target signals from interferents[212]. These capabilities are particularly relevant to sensor-integrated MPS, where biofouling, matrix-related interference, gradual baseline drift in culture conditions can compromise signal reliability.

AI may also facilitate the interpretation of high-dimensional and multimodal datasets generated by sensor-integrated MPSs. By integrating electrophysiological, mechanical, metabolic, barrier, and imaging data, machine-learning models may predict physiological states or response patterns that are not readily captured by individual sensing modalities alone[201, 202] . Recent studies further suggest that such data-driven approaches could be useful for predicting toxicity, drug resistance, and treatment responses in MPS models[213-215].

This type of data-driven interpretation could further be extended toward closed-loop operation, in which continuously acquired sensor signals are analyzed in real time and used to adjust experimental conditions such as perfusion, oxygen delivery, biochemical stimulation, or electrical stimulation[202, 214-216]. Although sensor-based feedback control has already been demonstrated in several MPS platforms, fully autonomous AI-assisted closed-loop operation remains at an early stage. Broader implementation will require representative training datasets, rigorous validation across different devices and experimental conditions, and interpretable models capable of distinguishing genuine biological changes from sensor-derived artifacts.

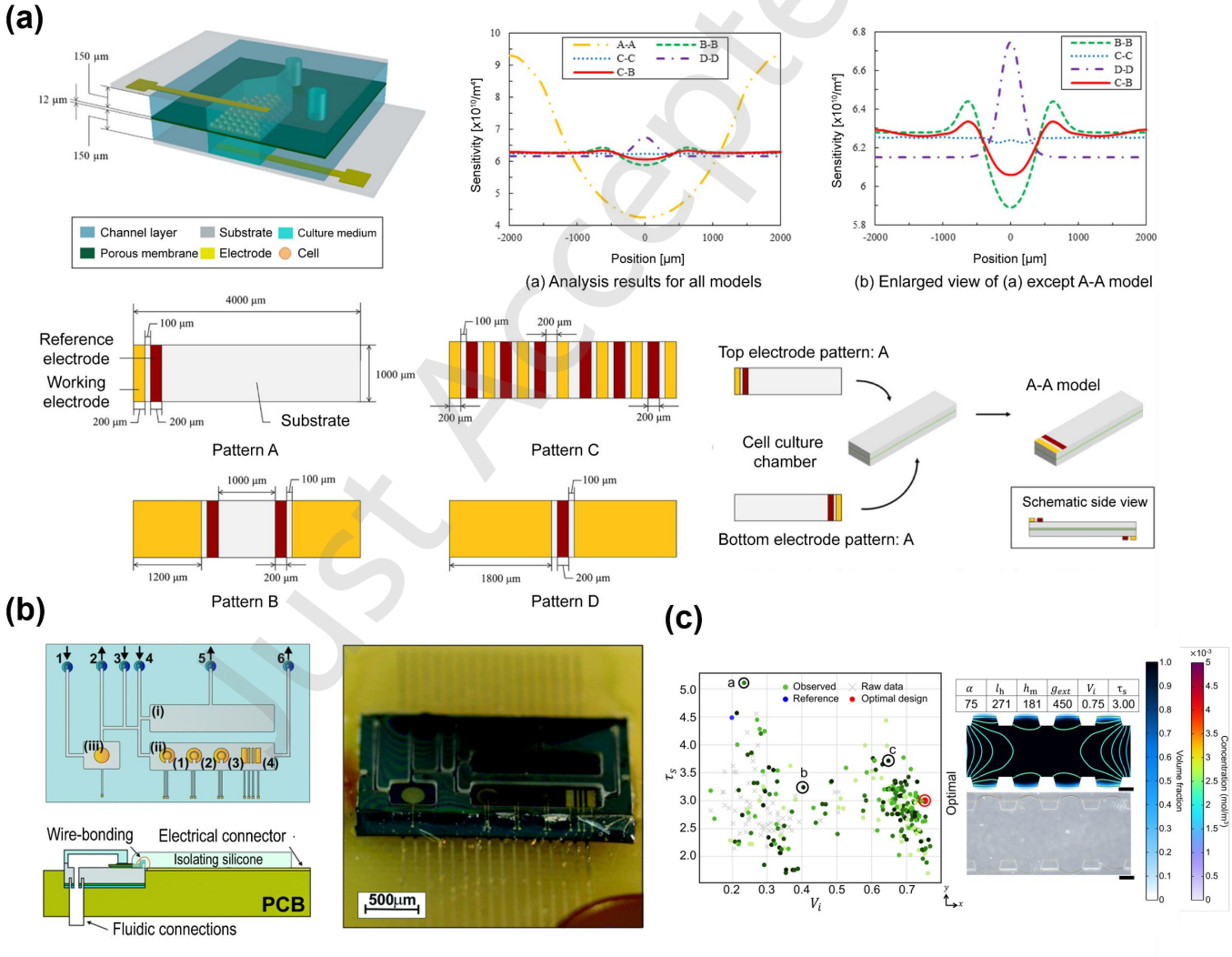


Figure 6 Key design considerations for sensor fabrication and integration in MPS.
(a) Computational optimal TEER electrode configurations through impedance sensitivity analysis, illustrating the influence of electrode configuration of measurement accuracy. Reproduced with permission from Ref. [57], © John Wiley & Sons Ltd 2021. (b) Multilayer sensor-integrated MPS architecture composed of heterogeneous materials, highlighting design considerations related to device bonding, assembly, and interfacial biocompatibility. Reproduced with permission from Ref. [192], © Royal Society of Chemistry 2020. (c) Example of an AI-assisted design workflow employing Bayesian optimization and computational

Just Accepted

simulations for microfluidic design optimization. Reproduced with permission from Ref. [204], © Royal Society of Chemistry 2026.; PCB: printed circuit board.

5 Conclusion and outlook

Recent advances in sensor integration technologies have substantially expanded the design space for sensing-enabled MPS, enabling quantitative and continuous monitoring of complex biological processes on-chip. In this review, we summarized sensing modalities, fabrication and integration strategies, and key design considerations that collectively determine the reliability and biological relevance of on-chip measurements. We first discussed how diverse physiological signals, including barrier integrity, mechanical forces, physical microenvironmental parameters, metabolic and biochemical microenvironment indicators, and electrophysiological activity, can be quantitatively monitored through advances in sensor technologies and system-level integration. We then reviewed bottom-up and top-down fabrication strategies for sensor-integrated MPSs. MEMS-based fabrication provides high precision, reproducibility, and circuit-level integration, while additive- and printing-based approaches enable rapid prototyping, material versatility, and low-cost manufacturing. Complementary top-down strategies, such as the integration of commercial sensing components and external electronics, further improve accessibility and reduce technical barriers. Importantly, these fabrication technologies are not mutually exclusive, rather, their convergence enables tailored solutions that balance resolution, scalability, and practical implementation. We further discussed key design considerations such as sensor placement, electrochemical behavior, biocompatibility, long-term stability, multimodal integration, sensor-selection frameworks, manufacturing constraints, and emerging AI-assisted strategies, that collectively shape the reliability and functionality of the sensor-integrated MPSs. Sensor-integrated MPSs provide a quantitative window into the dynamics of engineered microenvironments, enabling researchers to capture transient biochemical and biophysical events that traditional methods could not resolve.

Despite these advances, several fundamental challenges remain in sensor-integrated MPSs. First, spatially resolved monitoring within 3D tissues remains difficult, as sensors positioned at tissue surfaces or in perfusion channels may not capture local variations in oxygen levels, metabolite concentrations, or electrophysiological activity. Second, reliable continuous monitoring during long-term culture is often limited by biofouling, signal drift, and sensor degradation, which can compromise measurement accuracy over time. Third, integrating multiple sensing modalities within confined MPS geometries introduces challenges related to sensor placement, signal interference, and potential perturbations to fluid flow, molecular transport, and tissue organization. Addressing these challenges requires balancing measurement resolution, long-term stability, and preservation of physiological conditions, while ensuring reproducibility and scalability for broader implementation. Building on the developments discussed above, several emerging trends are expected to shape the next generation of sensor-integrated MPSs. While optical and electrochemical sensing modules have already been integrated into various MPS platforms, flexible, hybrid-fabricated, and wireless sensing technologies represent promising directions for broader implementation and improved long-term integration. Advances in materials, fabrication, and electronics have paved the way for the development of increasingly flexible, fully integrated, and wireless sensing systems. First, sensor technologies are likely to transition beyond rigid, planar substrates toward flexible and deformable architectures that better match the mechanical properties of living tissues. While silicon- and glass-based electrodes offer excellent precision, their mechanical mismatch with soft biological environments limits long-term integration, particularly in systems involving tissue motion or 3D constructs. Flexible sensors with low bending stiffness can mitigate these limitations, enhancing mechanical compatibility and measurement stability. Recent demonstrations in soft strain sensing and skin-mounted bioelectronics illustrate design principles that may be directly translated to MPSs requiring intimate tissue–sensor interfaces (**Fig. 7(a)**)[167, 217, 218].

Second, hybrid fabrication workflows that combine multiple fabrication technologies are expected to overcome current constraints in sensor integration. For example, integrating MEMS-based precision with additive manufacturing flexibility enables both microscale accuracy and rapid design customization. By leveraging the strengths of each approach including microscale accuracy, rapid customization, and cost efficiency, such hybrid strategies can enable multifunctional sensing architectures that are difficult to realize using a single fabrication paradigm alone (**Fig. 7(b)**)[219, 220]. In parallel, there is a clear transition from post-fabrication sensor attachment toward fully integrated workflows in which microfluidic structures and sensing elements are co-designed and co-fabricated from the outset (**Figs. 7(c)** and **7(d)**)[221]. Assembly-free and monolithic fabrication approaches reduce alignment errors, improve signal robustness, and offer scalable routes for reproducible MPS manufacturing.

Lastly, advances in wireless signal transmission and low-power electronics present important opportunities to further reduce wiring complexity and enhance system robustness. Because many sensing modalities ultimately transduce biological events into electrical signals, eliminating wired interconnects can reduce structural complexity, minimize leakage risks, and increase design flexibility. Recent examples of wireless microfluidic actuation and wearable electrochemical sensing illustrate the feasibility of such approaches and suggest a future in which MPSs incorporate fully embedded, wireless sensing modules for long-term, minimally perturbative monitoring[222].

Continued innovation at the convergence of materials science, microfabrication, electronics, and data-driven design is expected to drive the development of increasingly quantitative, scalable, and physiologically reliable MPSs with integrated sensing capabilities. Ultimately, sensor selection and integration should be guided by the physiological signals of interest and their spatial and temporal characteristics, rather than by sensing performance or fabrication convenience alone. Balancing

Just Accepted

measurement reliability, biological compatibility, long-term stability, and manufacturability will be essential for the broader implementation of sensor-integrated MPSs. These advances will deepen our understanding of complex biological systems while accelerating the translation of MPS technologies into drug development, disease modeling, and personalized medicine.

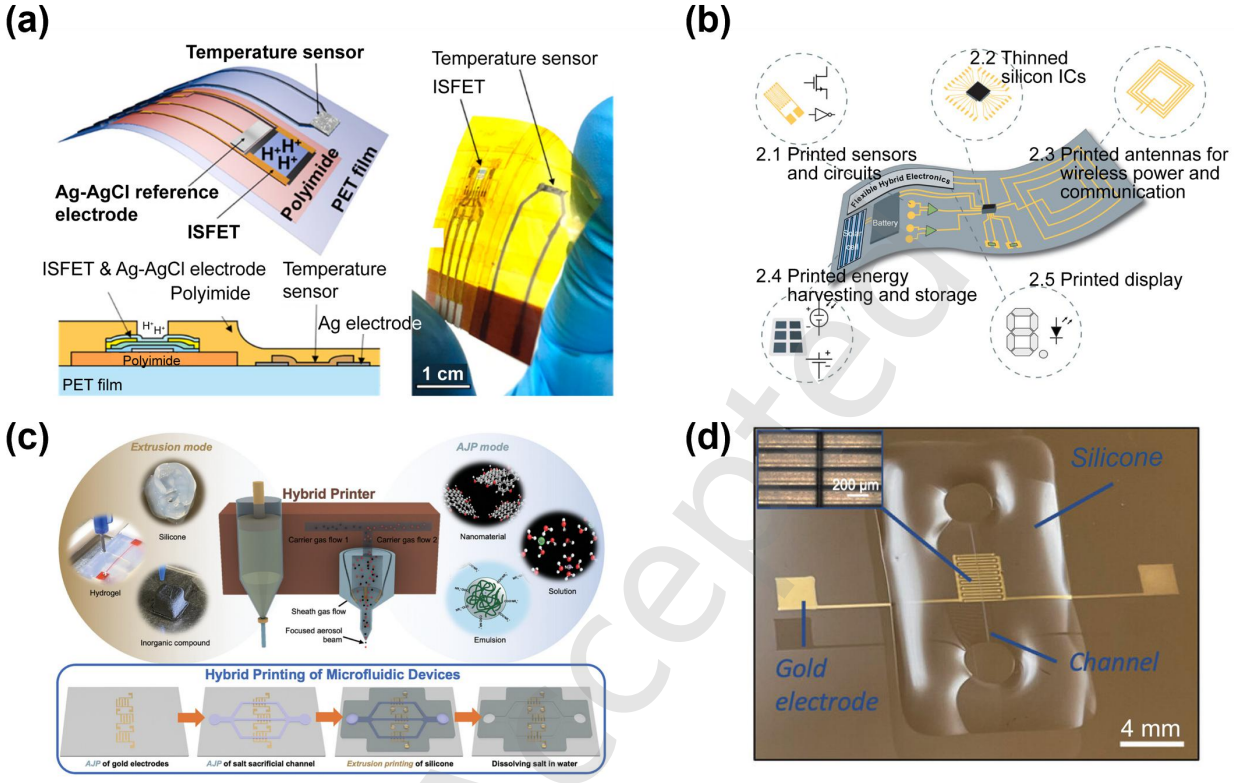


Figure 7 Future directions in sensor fabrication and integration for next-generation MPS.

(a) Flexible and skin-mounted bioelectronic sensors as design inspiration for future sensor-integrated MPSs. Reproduced with permission from Ref. [217], © American Chemical Society 2017. (b) Hybrid fabrication workflows combining MEMS processing with printed electronics for multifunctional sensing systems. Reproduced with permission from Ref. [219], © The Authors. Advanced Materials published by Wiley-VCH GmbH 2022. (c) Hybrid printing strategy enabling fabrication of fully integrated MPSs with heterogeneous materials and multiscale features without post-assembly processes. Reproduced with permission from Ref. [221], © Wiley-VCH GmbH 2023. (d) Example of a fully integrated electrochemical sensing platform fabricated through hybrid printing of microfluidic structures and functionalized Au electrodes. Reproduced with permission from Ref. [221], © Wiley-VCH GmbH 2023.; ISFET: ion-sensitive field-effect transistor; PET: polyethylene terephthalate; IC: integrated circuit; AJP: aerosol jet printing.

Table 1. Summary of major sensing technologies for physiological monitoring in MPSs

Sensing target	Representative sensing technology	Sensing principle	Advantages	Limitations	Representative MPS applications
Barrier integrity	TEER / impedance spectroscopy	Electrical resistance or impedance across a cellular barrier using two- or four-electrode configurations	Label-free; continuous monitoring; non-destructive	Sensitive to electrode configuration, polarization, current-path geometry, and sensing area	Tissue barrier models including vascular barrier model[156], blood-brain barrier models[18, 51] , bronchial barrier model[61], and intestinal barrier model[64]
Mechanical responses	Strain/resistive sensors	Changes in electrical resistance change	Real-time and label-free measurement;	Requires mechanical coupling; sensor	Cardiac muscle models[75], breathing lung model[72]

Just Accepted

		induced by mechanical deformation	compatible with dynamic stimulation	stiffness and placement may perturb tissue mechanics; calibration can be geometry-dependent	
Physical microenvironment	Pressure sensors	Piezoresistive or capacitive signals generated by membrane deformation	Direct in situ monitoring of local pressure; suitable for dynamic pressure changes	Sensor insertion may perturb flow; packaging and spatial placement are critical	Kidney/glomerularmode[88], vascular endothelial model[80], and perfused OoC model[91]
	Flow sensors	Thermal, mechanical, optical, or mass-flow transduction	Enables direct monitoring of perfusion conditions and detection of flow disturbances such as blockage/leakage	Added fluidic resistance/dead volume; external or in-line sensors may not represent local cell-level conditions	Perfused single- and multi-organ chips; automated flow-control systems[90, 91]
Metabolic microenvironment	Optical O_2/ pH sensors	Optical response of indicator dyes	Non-invasive; electrically isolated from the culture environment; compatible with spatial mapping	Photobleaching, optical interference, calibration requirements, and dependence on optical instrumentation	Metabolic monitoring in tumor model[120], liver models[111, 116], cardiac models[119, 186], multi-organ MPSs[199]
	Electrochemical metabolite sensors	Electrochemical detection of metabolites	High sensitivity; suitable for continuous or real-time monitoring	Biofouling, enzyme degradation, signal drift during long-term culture	Glucose/lactate monitoring in liver models[195, 197], tumor model[120], muscle model[102], and multi-organ MPSs[121, 122]
Electrophysiological activity	Microelectrode arrays (MEAs)	Extracellular recording of field potentials	Label-free, high temporal resolution and spatially resolved measurements	Signal quality depends on cell–electrode coupling; limited primarily to electrically active tissues	Electrically active tissue models including cardiac model[125], neural model[126] and pancreatic islet MPS[127]

TEER: trans-endothelial/epithelial electrical resistance; MEA: microelectrode array; BBB; blood–brain barrier; OoC: organ-on-a-chip; ~~₩~~

Table 2. MEMS-based fabrication sensor integration into MPSs

Sensing parameter	Sensor materials	Sensor characteristics	Sensor dimensions	Fabrication method	Ref
Barrier integrity (TEER)	Au (electrode) PC (substrate)	Optical transparency Frequency: 530 Hz with an amplitude of 5 mV_{RMS}	Thickness: 18 nm	Sputtering	[54]
Barrier integrity (TEER)	Au, Ti (electrode) PC (substrate)	4-point measurement Frequency range: 10 Hz -	Width: 1 mm Spacing: 1 mm	E-beam evaporation	[56]

Just Accepted

		100 kHz			
Barrier integrity (TEER)	Ti, Pt (electrode) Pt black (surface treatment) Borosilicate glass, SiO_2 (substrate)	Multifunctional monitoring Frequency range: 1 - 10 kHz Neural recording (EAP and LFP measurement)	Width: 40 μm Length: 4 mm (TEER electrode) Size: 50*50 μm, 24 arrays (RE)	Photolithography E-beam evaporation Lift-off	[60]
Barrier integrity (TEER)	Ag wire (electrode) ITO (MEA) Glass (substrate)	Multimodal sensing Optical transparency Frequency: 10 kHz (maximum)	Width: 100 μm (TEER electrode) Array: 8 - 16 (MEA)	Photolithography Sputtering Wet etching	[61]
Barrier integrity (TEER)	Ag/AgCl wire (electrode) ITO (MEA) Glass (substrate)	Combined sensing Frequency range: 10 Hz - 1 kHz (TEER), - 10 kHz (MEA)	Width: 100 μm Array: 12 - 16 (MEA)	Photolithography E-beam evaporation Lift-off	[62]
Barrier integrity (TEER)	ITO (electrode) Glass (substrate)	Impedance spectroscopy Frequency range: 10 Hz - 1 MHz 4-point arrangement, 2 pair	-	Photolithography Sputtering Lift-off	[64]
Barrier integrity (TEER)	Pt (electrode) Glass or PI (substrate)	Cu layer, electroless Ni plating and immersion of Au layer	Thickness: 35 μm, 50 nm (Cu, Au)	Electroless plating	[72]
Barrier integrity (TEER)	Au, Stainless steel wire (electrode)	Spatial resolution Frequency range: 1 Hz - 1 MHz	Diameter: 0.5 mm (wire, top) Width: 2 mm Spacing: 0.5 mm (bottom)	Sputtering	[150]
Barrier integrity (TEER)	Ag/AgCl thin film (electrode) Glass and PDMS (substrate)	4-point analysis optical imaging compatibility Surface treatment with $FeCl_3$	Thickness: 800 nm (Ag) Spacing: 200 μm	Sputtering	[151]
Barrier integrity (TEER)	Ti, Au (electrode) ITO (MEA) PC (substrate)	Multimodal measurements 4-point impedance analysis	Spacing: 1mm Thickness: 3 nm, 25 nm (Ti, Au, TEER electrode) Width: 100 μm Thickness: 100 nm Spacing: 100 μm (MEA)	Photolithography E-beam evaporation ICP etching	[155]
Barrier integrity (TEER)	Au (electrode) Soda lime glass (substrate)	Square wave voltammetry	Thickness: 100 nm Spacing: 1 mm	Photolithography Wet etching	[156]
Barrier integrity (TEER), Electrophysiological	Au (electrode) OSTE+ (substrate)	Optical transparency Frequency range: 10 Hz - 100 kHz	Thickness: 100 nm Width: 1 mm Length: 100 μm	Photolithography Sputtering	[59]

Just Accepted

activity (impedance)		Continuous measurement at < 2 min intervals			
Barrier integrity (TEER), Electrophysiological activity (cell capacitance)	Ti, Au (electrode) PC (substrate)	Multimodal sensing Frequency range: 10 Hz - 100 kHz	Thickness: 1 mm Length: 1 mm Spacing: 1 mm	Photolithography E-beam evaporation Wet etching.	[152]
Electrophysiological activity (impedance)	Au (electrode) OSTE+, PDMS (flexible substrate) Glass (rigid substrate)	Frequency range: 10 Hz - 100 kHz Substrate compatibility	Thickness: 100 nm Width: 100 µm Spacing: 50 µm	E-beam evaporation Sputtering	[156]
Electrophysiological activity (beat frequency, signal propagation rate, action potential)	Ti, Au (electrode) Glass (substrate)	Non-invasive monitoring Frequency range: 10 Hz - 1 MHz Optical transparency imaging 4-point arrangement	Thickness: 20 nm, 80 nm (Ti, Au)	Photolithography Sputtering Wet etching	[125]
Electrophysiological activity (biomarker monitoring)	Au (WE, CE) Ag (RE) Glass (substrate)	Label free detection Multiplex biomarker sensing Automatic system Regenerability	Thickness: 500 nm Width: 800 µm Spacing: 200 µm (WE) Thickness: 500 nm Width: 150 µm (CE) Thickness: 500 nm (RE)	E-beam evaporation	[153]
Electrophysiological activity (impedance)	Au (electrode) PDMS (substrate)	Stretchable sensor Impedance spectroscopy	Diameter: 200 µm (WE) Area: 0.36cm^2 (CE) 60*44*2 mm (substrate)	Sputtering ICP etching	[158]
Electrophysiological activity (ECIS)	Au, Ti (electrode) Glass (substrate)	Distance-dependent sensing	Thickness: 25 nm, 50 nm (Ti, Au) Diameter: 100 µm Distance from confrontation line: 100 - 3050 µm	Photolithography E-beam evaporation Lift off	[159]
Electrophysiological activity (conduction velocity)	Pt (MEA) Stainless steel wire (stimulation electrode) Fused silica (substrate)	Multi organ integration (heart, liver)	Diameter: 80 µm Spacing: 10 mm Array: 2*5 (MEA)	Photolithography E-beam evaporation DRIE	[160]
Metabolic microenvironment indicators (pH),	P-type Si wafer (substrate) Thermally grown	Multi-modal sensing	Size: 1 cm^2 Thickness: 100 nm (gate oxide)	Photolithography Ion implantation PECVD	[161]

Just Accepted

Electrophysiological activity (action potential)	oxide layer (gate) AlSi (conductors and floating gate) PECVD oxide (interlayer dielectric) PI (insulation and mechanical transfer layer) Ti (control gate electrode)		Thickness: 1 μm, 300 nm (AlSi, Ti, electrode) Thickness: 150 nm (inter-gate dielectric)	Sputtering DRIE	
Mechanical properties (strain gage)	Ti, Au (electrode) Glass (substrate)	Non-invasive real-time monitoring Parallel measurement Tissue geometry control 4-point arrangement.	Thickness: 20 nm, 80 nm (Ti, Au)	E-beam evaporation	[75]
Mechanical properties (strain gage)	Ti (metal strain gage) PEDOT:PSS (polymer strain gage) Al, Ag (electrical contact) PDMS (substrate)	Real-time monitoring, Monolithic microfabrication Radial and tangential structure Humidity stability	Thickness: 100 nm, 600 nm, 100 nm (electrode, Ti, Al, Ag) Thickness: 20 μm (gage)	Photolithography PECVD DRIE ICP etching Sputtering Wet etching	[157]
Temperature	Double-side polished p-type Si wafer (substrate) P-type epitaxial layer (epitaxial layer) SiO_2 (gate dielectric) AlSi (interconnect and gate electrode, contact pad, membrane electrode) SiO_2 (capacitor dielectric)	Microfabrication compatible Circuit structure: NPN bipolar transistor, NMOS/PMOS transistor, MIM capacitor	Area: 49 mm^2	Photolithography Ion implantation Sputtering DRIE	[162]

OSTE+: off-stoichiometry thiol-ene-epoxy; E-beam: electron-beam; BBB: blood-brain barrier; DRIE: deep reactive-ion etching; PECVD: plasma enhanced chemical vapor deposition; ICP: inductively coupled plasma; PC: polycarbonate; PI: polyimide; PDMS: polydimethylsiloxane; PTFE: polytetrafluoroethylene; EAP: extracellular action potential; LFP: local field potential; ITO: indium tin oxide; WE: working electrode; CE: counter electrode; RE: reference electrode; MEA: multi-electrode array; TEER: transendo/epithelial electrical resistance; PEDOT:PSS: Poly(2,3-dihydrothieno-1,4-dioxin)-poly(styrenesulfonate); MIM: metal-insulator-metal.

Table 3. Representative printing-based approaches for sensor integration into MPSs

Sensing parameter	Sensor materials	Sensor characteristics	Sensor dimensions	Fabrication method	Ref
Metabolic	Au, Ag (conductive	Spatial resolution	Width: 300 μm	Inkjet printing	[163]

Just Accepted

microenvironment indicators (oxygen gradient)	ink) PTFE (substrate)		Pattern resolution: 1693 dpi		
Metabolic microenvironment indicators (oxygen gradient)	Au, Ag (conductive ink) Soda lime glass (substrate)	Multimodal sensing Spatial resolution Layered electrode structure	Thickness: 300 nm	Inkjet printing	[165]
Barrier integrity (TEER), bubble detection	Conductive carbon, Ag (conductive ink) PET (substrate)	Frequency range: 10 Hz - 100 kHz Bubble detection	Thickness: 10 - 15 µm Area: 1 mm^2 Spacing: 2 mm	Screen printing	[58]
Barrier integrity (TEER)	Ag/AgCl (conductive ink) PET (substrate)	4-point arrangement	Thickness:10 - 20 µm	Screen printing	[164]
Metabolic microenvironment indicators (oxygen gradient)	Rt complex (oxygen sensor) PS (substrate)	Fluorescence quenching sensing Polymer fiber-based sensor	-	Spray printing	[178]
Metabolic microenvironment indicators (oxygen gradient)	PtTPTBPF (oxygen sensor) Silicon and borosilicate glass (substrate)	Luminescence lifetime-based phase shift sensing	Diameter: 100 µm	Spray printing	[166]
Electrophysiological activity / Mechanical properties (contractile force)	PEDOT:PSS (3D microelectrode) TPE/QD nanocomposite (force sensor) Au/Ti-coated glass (substrate)	Multimodal sensing; extracellular field potential and contractile force monitoring; soft tissue-interfacing electrodes	Diameter: 5 ± 0.5 µm Height: 250 ± 10 µm (PEDOT:PSS pillar) Spacing: 100 µm	Meniscus-guided direct writing / Extrusion-based 3D printing	[223]
Electrophysiological activity	EGaIn (liquid-metal electrode) Pt nanoclusters (surface treatment) Parylene-C (passivation)	Soft 3D intra-organoid recording; electrophysiological monitoring during temporal interference stimulation; 60-electrode MEA	Diameter: 18 µm Height: 250 µm (3D LM pillar)	Direct 3D liquid-metal printing	[169]
Electrophysiological activity	EGaIn (liquid-metal electrode) Pt nanoclusters (surface treatment) Parylene-C (passivation)	3D intra-organoid recording; mechanically soft and magnetically reshapable electrodes	Diameter: ≥14 µm Height: >310 µm (3D LM pillar)	Direct 3D liquid-metal printing	[170]
Mechanical properties (contractile stress)	CB:TPU (piezoresistive	Continuous electronic monitoring of cardiac	Thickness: 6.5 µm (strain sensor) 3 µm (TPU base)	Multimaterial DIW 3D printing	[167]

Just Accepted

	strain sensor) Ag:PA (interconnect) TPU/PDMS (device structure)	contractile stress; integrated soft strain gauge	1.5 μm (wire cover)		
Cellular response (impedance)	PEDOT:PSS/PEGDA (conductive hydrogel electrode) GelMA (cell-laden hydrogel)	Label-free EIS monitoring; discrimination of cell density and spheroid size	Layer thickness: 100 μm	Multimaterial DLP 3D bioprinting	[224]
Electrical stimulation	PEDOT:PSS (3D pillar electrode) Au (underlying electrode) PDMS (chamber)	3D electrical stimulation of neural tissues	Diameter: 14 ± 1 μm Height: 80 ± 2 μm	Direct-write printing	[225] †
Barrier integrity (TEER)	Au (electrode) Ti (adhesion layer) Glass / SLA-printed resin (substrate)	4-point TEER; non-invasive real-time monitoring; optical accessibility; commercial EVOM compatibility	Thickness: 50 nm Au + 100 nm Ti (glass) 100 nm Au (3D-printed component)	SLA 3D printing + PVD sputtering	[226] ‡
Mechanical properties (contractile force)	TPE/QD nanocomposite (force sensor) PS (substrate) Carbon (stimulation electrode)	Fluorescent displacement-based force sensing; scalable multiwell format; long-term electrical conditioning	Diameter: 60 μm (TPE/QD microwire)	Extrusion-based 3D printing + hot embossing	[168]

PTFE: polytetrafluoroethylene; PET: Polyethylene terephthalate; TEER: transendo/epithelial electrical resistance; PS: polystyrene; PtTPTBPF: platinum(II)-5,10,15,20-tetrakis(2,3,4,5,6-pentafluorophenyl)porphyrin tetrabenzoporphyrin.; PEDOT:PSS: poly(3,4-ethylenedioxythiophene):poly(styrene sulfonate); TPE: thermoplastic elastomer; QD: quantum dot; EGaIn: eutectic gallium–indium; LM: liquid metal; MEA: multi-electrode array; CB:TPU: carbon black-filled thermoplastic polyurethane; Ag:PA: silver particle-filled polyamide; PEGDA: polyethylene glycol diacrylate; GelMA: gelatin methacryloyl; EIS: electrochemical impedance spectroscopy; DIW: direct ink writing; DLP: digital light processing; SLA: stereolithography; PVD: physical vapor deposition; PDMS: polydimethylsiloxane.

Data availability

Not applicable.

Acknowledgements

This work was supported by the National Research Foundation of Korea (NRF) grant funded by the Korea government (MSIT) (No. RS-2026-25487930); and by a grant of the Korea-US Collaborative Research Fund(KUCRF), funded by the Ministry of Science and ICT and Ministry of Health & Welfare, Republic of Korea (No. RS-2024-00468873); and by the Technology Innovation Program (RS-2024–00448758) funded by the Ministry of Trade, Industry & Energy (MOTIE, Republic of Korea)

Declaration of competing interest

All the contributing authors report no conflict of interest in this work.

Author contribution statement

S. M.: Writing – original draft, review & editing, investigation, conceptualization, visualization, software. J. S. C.: Writing – original draft, review & editing, investigation, N. K.: Writing - review & editing, visualization, software, S. I.: Writing – original draft, review & editing, conceptualization, funding acquisition.

Just Accepted

CRediT author statement (https://credit.niso.org/) is recommended to use, and all the listed authors should meet the definition of Author in ICMJE recommendations (https://www.icmje.org/).

Informed consent
Not applicable.

Ethics statement
Not applicable

Use of AI statement
None.

References

[1] Reyes, D. R.;Esch, M. B.;Ewart, L.;Nasiri, R.;Herland, A.;Sung, K.;Piergiovanni, M.;Lucchesi, C.;Shoemaker, J. T.; Vukasinovic, J. From animal testing to in vitro systems: advancing standardization in microphysiological systems. *Lab Chip* **2024**, *24*, 1076–1087.

[2] Wu, Q.;Liu, J.;Wang, X.;Feng, L.;Wu, J.;Zhu, X.;Wen, W.; Gong, X. Organ-on-a-chip: recent breakthroughs and future prospects. *Biomed. Eng. Online* **2020**, *19*, 9.

[3] Ravi, M.;Paramesh, V.;Kaviya, S.;Anuradha, E.; Solomon, F. P. 3D cell culture systems: advantages and applications. *J. Cell. Physiol.* **2015**, *230*, 16–26.

[4] Evans, H. J.;Sweet, J. K.;Price, R. L.;Yost, M.; Goodwin, R. L. Novel 3D culture system for study of cardiac myocyte development. *Am. J. Physiol. Heart Circul. Physiol.* **2003**, *285*, H570–H578.

[5] Ader, M.; Tanaka, E. M. Modeling human development in 3D culture. *Curr. Opin. Cell Biol.* **2014**, *31*, 23–28.

[6] Langhans, S. A. Three-dimensional in vitro cell culture models in drug discovery and drug repositioning. *Front. Pharmacol.* **2018**, *9*, 6.

[7] Leung, C. M.;de Haan, P.;Ronaldson-Bouchard, K.;Kim, G.-A.;Ko, J.;Rho, H. S.;Chen, Z.;Habibovic, P.;Jeon, N. L.;Takayama, S.;Shuler, M. L.;Vunjak-Novakovic, G.;Frey, O.;Verpoorte, E.; Toh, Y.-C. A guide to the organ-on-a-chip. *Nat. Rev. Methods Prim* **2022**, *2*, 33.

[8] Cho, S.;Lee, S.; Ahn, S. I. Design and engineering of organ-on-a-chip. *Biomed. Eng. Lett.* **2023**, *13*, 97–109.

[9] Ferrari, E.;Nebuloni, F.;Rasponi, M.; Occhetta, P. Photo and soft lithography for organ-on-chip applications. In *Organ-on-a-chip: methods and protocols*. M. Rasponi, Ed.; Humana; New York, 2021; pp 1–19.

[10] Yi, H.-G.;Jeong, Y. H.;Kim, Y.;Choi, Y.-J.;Moon, H. E.;Park, S. H.;Kang, K. S.;Bae, M.;Jang, J.; Youn, H. A bioprinted human-glioblastoma-on-a-chip for the identification of patient-specific responses to chemoradiotherapy. *Nat. Biomed. Eng.* **2019**, *3*, 509–519.

[11] Park, J. Y.;Ryu, H.;Lee, B.;Ha, D.-H.;Ahn, M.;Kim, S.;Kim, J. Y.;Jeon, N. L.; Cho, D.-W. Development of a functional airway-on-a-chip by 3D cell printing. *Biofabrication* **2018**, *11*, 015002.

[12] Kim, J.;Yoon, T.;Kim, P.;Bekhbat, M.;Kang, S. M.;Rho, H. S.;Ahn, S. I.; Kim, Y. Manufactured tissue-to-tissue barrier chip for modeling the human blood–brain barrier and regulation of cellular trafficking. *Lab Chip* **2023**, *23*, 2990–3001.

[13] Hosic, S.;Bindas, A. J.;Puzan, M. L.;Lake, W.;Soucy, J. R.;Zhou, F.;Koppes, R. A.;Breault, D. T.;Murthy, S. K.; Koppes, A. N. Rapid Prototyping of Multilayer Microphysiological Systems. *ACS Biomater. Sci. Eng.* **2021**, *7*, 2949–2963.

[14] Sabate Del Rio, J.;Ro, J.;Yoon, H.;Park, T. E.; Cho, Y. K. Integrated technologies for continuous monitoring of organs-on-chips: Current challenges and potential solutions. *Biosens. Bioelectron.* **2023**, *224*, 115057.

[15] Jones, C. G.; Chen, C. A customizable continuous and near real-time TEER platform to study anti-cancer drug toxicity in barrier tissues. *J. Pharm. Anal.* **2025**, *15*, 101266.

[16] Bavli, D.;Prill, S.;Ezra, E.;Levy, G.;Cohen, M.;Vinken, M.;Vanfleteren, J.;Jaeger, M.; Nahmias, Y. Real-time monitoring of metabolic function in liver-on-chip microdevices tracks the dynamics of mitochondrial dysfunction. *Proc. Natl. Acad. Sci. U. S. A.* **2016**, *113*, E2231–E2240.

[17] Yang, J. W.;Khorsandi, D.;Trabucco, L.;Ahmed, M.;Khademhosseini, A.;Dokmeci, M. R.;Ye, J. Y.; Jucaud, V. Liver-on-a-Chip Integrated with Label-Free Optical Biosensors for Rapid and Continuous Monitoring of Drug-Induced Toxicity. *Small* **2024**, *20*, e2403560.

[18] Ryoo, M.;Lee, G.;Jung, J.;Cho, S.;Ham, S. J.;Kang, N.;Ahn, H.;Kim, Y. J.;Sim, J.;Park, J.;Kim, J.;Hwang, S.;Yoo, J.;Kang, Y. J.;Lim, J.;Ahn, J.; Ahn, S. I. Human Blood-Brain Tumor Barrier on a Chip to Investigate Personalized Treatment for Glioblastoma Patients. *Small* **2026**, *22*, e06712.

[19] Kalejaiye, T. D.;Bhattacharya, R.; Musah, S. A Vascularized Human Organ Chip Reveals SARS-CoV-2 Susceptibility in Developmentally Guided Tissue Maturation. *Cel. Mol. Bioeng.* **2025**, *18*, 453–471.

[20] Maoz, B. M.;Herland, A.;FitzGerald, E. A.;Grevesse, T.;Vidoudez, C.;Pacheco, A. R.;Sheehy, S. P.;Park, T. E.;Dauth, S.;Mannix, R.;Budnik, N.;Shores, K.;Cho, A.;Nawroth, J. C.;Segre, D.;Budnik, B.;Ingber, D. E.; Parker, K. K. A linked organ-on-chip model of the human neurovascular unit reveals the metabolic coupling of endothelial and neuronal cells. *Nat. Biotechnol.* **2018**, *36*, 865–874.

[21] Tataru, C.;Livni, M.;Marean-Reardon, C.;Franco, M. C.; David, M. Cytokine induced inflammatory bowel disease model using organ-on-a-chip technology. *PLoS One* **2023**, *18*, e0289314.

[22] Kerns, S. J.;Belgur, C.;Petropolis, D.;Kanellias, M.;Barrile, R.;Sam, J.;Weinzierl, T.;Fauti, T.;Freimoser-Grundschober, A.;Eckmann, J.;Hage, C.;Geiger, M.;Ng, P. R.;Tien-Street, W.;Manatakis, D. V.;Micallef, V.;Gerard, R.;Bscheider, M.;Breous-Nystrom, E.;Schneider, A.;Giusti, A. M.;Bertinetti-Lapatki, C.;Grant, H. S.;Roth, A. B.;Hamilton, G. A.;Singer, T.;Karalis, K.;Moisan, A.;Bruenker, P.;Klein, C.;Bacac, M.;Gjorevski, N.; Cabon, L. Human immunocompetent Organ-on-Chip platforms allow safety profiling of tumor-targeted T-cell bispecific antibodies. *Elife* **2021**, *10*.

[23] Shen, H.;Li, Q.;Song, W.; Jiang, X. Microfluidic on-chip valve and pump for applications in immunoassays. *Lab Chip* **2023**, *23*, 341–348.

[24] Ntziachristos, V. Going deeper than microscopy: the optical imaging frontier in biology. *Nat. Methods* **2010**, *7*, 603–614.

[25] Choi, D. S.;Lim, S.;Park, J.-S.;Kim, C.-H.;Rhee, H.; Cho, M. Label-free live-cell imaging of internalized microplastics and

Uncorrected

cytoplasmic organelles with multicolor CARS microscopy. *Environ. Sci. Technol.* **2022**, *56*, 3045–3055.
[26] Peel, S.; Jackman, M. Imaging microphysiological systems: a review. *Am. J. Physiol. Cell Physiol.* **2021**, *320*, C669–C680.
[27] van der Helm, M. W.;Odijk, M.;Frimat, J.-P.;van der Meer, A. D.;Eijkel, J. C.;van den Berg, A.; Segerink, L. I. Direct quantification of transendothelial electrical resistance in organs-on-chips. *Biosens. Bioelectron.* **2016**, *85*, 924–929.
[28] Vera, D.;García-Díaz, M.;Torras, N.;Castillo, Ó.;Illa, X.;Villa, R.;Alvarez, M.; Martinez, E. A 3D bioprinted hydrogel gut-on-chip with integrated electrodes for transepithelial electrical resistance (TEER) measurements. *Biofabrication* **2024**, *16*, 035008.
[29] Bossink, E. G. B. M.;Zakharova, M.;de Bruijn, D. S.;Odijk, M.; Segerink, L. I. Measuring barrier function in organ-on-chips with cleanroom-free integration of multiplexable electrodes. *Lab Chip* **2021**, *21*, 2040–2049.
[30] Vila, O. F.;Chavez, M.;Ma, S. P.;Yeager, K.;Zholudeva, L. V.;Colón-Mercado, J. M.;Qu, Y.;Nash, T. R.;Lai, C.; Feliciano, C. M. Bioengineered optogenetic model of human neuromuscular junction. *Biomaterials* **2021**, *276*, 121033.
[31] Gaio, N.;Waafi, A.;Vlaming, M.;Boschman, E.;Dijkstra, P.;Nacken, P.;Braam, S.;Boucsein, C.;Sarro, P.; Dekker, R. A multiwell plate Organ-on-Chip (OOC) device for in-vitro cell culture stimulation and monitoring. In *2018 IEEE Micro Electro Mechanical Systems (MEMS)*; IEEE; Piscataway, NJ, USA, 2018; pp 314–317.
[32] Mastrangeli, M.;Aydogmus, H.;Dostanic, M.;Motreuil-Ragot, P.;Revyn, N.;De Wagenaar, B.;Dekker, R.; Sarro, P. M. Microelectromechanical organs-on-chip. In *2021 21st International Conference on Solid-State Sensors, Actuators and Microsystems (Transducers)*; IEEE; Orlando, FL, USA, 2021; pp 102–107.
[33] Dey, S.;Kinoshita, M.;Puttick, S.;Rose, S.;Trau, M.;Roberts, M. J.; Koo, K. M. Cancer‐on‐Chip and Integrative Tumor Microenvironment Sensor Technologies for Progressing Precision Radiotherapy. *Adv. Sensor Res.* **2024**, *3*, 2300193.
[34] Fuchs, S.;Johansson, S.;Tjell, A. Ø.;Werr, G.;Mayr, T.; Tenje, M. In-line analysis of organ-on-chip systems with sensors: Integration, fabrication, challenges, and potential. *ACS Biomater. Sci. Eng.* **2021**, *7*, 2926–2948.
[35] Zhu, Y.;Mandal, K.;Hernandez, A. L.;Kawakita, S.;Huang, W.;Bandaru, P.;Ahadian, S.;Kim, H.-J.;Jucaud, V.;Dokmeci, M. R.; Khademhosseini, A. State of the art in integrated biosensors for organ-on-a-chip applications. *Curr. Opin. Biomed. Eng.* **2021**, *19*.
[36] Hussain Memon, F.;Inseok, K.;Ahmed, F.;Ali, W.;Soomro, A. M.;Raza Memon, S.;Hussain Memon, K.; Choi, K. H. A Comprehensive Review of Biosensor Integration in Microphysiological Systems for Online Monitoring: Current Challenges and Future Advancements. *ChemBioEng Reviews* **2023**, *10*, 817–828.
[37] Casanova, A.;Alimohammadzadeh, E.;McCormirk, S.;Thomas, Y. R. J.;Den Dulk, R.;Baldi, A.;Fernández-Sánchez, C.;Ghaemmaghami, A. M.; Mailley, P. Integration of electrochemical sensors in organ-on-a-chip microfluidic platforms: Advances and perspectives. *Biosens. Bioelectron.* **2026**, *311*.
[38] Cognetti, J. S.; Miller, B. L. Real-Time, Continuous Monitoring of Tissue Chips as an Emerging Opportunity for Biosensing. *Sensors* **2025**, *25*.
[39] Ling, S.;Xu, C.;Jiang, Y.;Xu, F.;Jin, H.;Chen, H.;Chen, S.;Ding, Z.; Sun, D. Toward continuous monitoring systems: emerging trends of on-chip sensors in organ-on-a-chip. *Microsyst. Nanoeng.* **2026**, *12*.
[40] Tawade, P.; Mastrangeli, M. Integrated Electrochemical and Optical Biosensing in Organs‐on‐Chip. *ChemBioChem* **2023**, *25*.
[41] Mou, L.;Mandal, K.;Mecwan, M. M.;Hernandez, A. L.;Maity, S.;Sharma, S.;Herculano, R. D.;Kawakita, S.;Jucaud, V.;Dokmeci, M. R.; Khademhosseini, A. Integrated biosensors for monitoring microphysiological systems. *Lab Chip* **2022**, *22*, 3801–3816.
[42] Chen, H.;Luo, Z.;Lin, X.;Zhu, Y.; Zhao, Y. Sensors-integrated organ-on-a-chip for biomedical applications. *Nano Res.* **2023**, 1–28.
[43] Yang, W.;Li, T. Y.;Liao, S. F.;Zhou, J. H.; Huang, L. Organ-on-a-chip platforms integrated with biosensors for precise monitoring of the cells and cellular microenvironment. *TrAC - Trends Anal. Chem.* **2024**, *172*.
[44] Walter, F. R.;Valkai, S.;Kincses, A.;Petneházi, A.;Czeller, T.;Veszelka, S.;Ormos, P.;Deli, M. A.; Dér, A. A versatile lab-on-a-chip tool for modeling biological barriers. *Sens. Actuators B: Chem.* **2016**, *222*, 1209–1219.
[45] Niec, R. E.;Rudensky, A. Y.; Fuchs, E. Inflammatory adaptation in barrier tissues. *Cell* **2021**, *184*, 3361–3375.
[46] Ugodnikov, A.;Persson, H.; Simmons, C. A. Bridging barriers: advances and challenges in modeling biological barriers and measuring barrier integrity in organ-on-chip systems. *Lab Chip* **2024**, *24*, 3199–3225.
[47] Srinivasan, B.;Kolli, A. R.;Esch, M. B.;Abaci, H. E.;Shuler, M. L.; Hickman, J. J. TEER measurement techniques for in vitro barrier model systems. *J. Lab. Autom.* **2015**, *20*, 107–126.
[48] Malik, M.;Steele, S. A.;Mitra, D.;Long, C. J.; Hickman, J. J. Trans-epithelial/endothelial electrical resistance (TEER): Current state of integrated TEER measurements in organ-on-a-chip devices. *Curr. Opin. Biomed. Eng.* **2025**, *34*, 100588.
[49] Nazari, H.;Shrestha, J.;Naei, V. Y.;Bazaz, S. R.;Sabbagh, M.;Thiery, J. P.; Warkiani, M. E. Advances in TEER measurements of biological barriers in microphysiological systems. *Biosens. Bioelectron.* **2023**, *234*, 115355.
[50] Douville, N. J.;Tung, Y.-C.;Li, R.;Wang, J. D.;El-Sayed, M. E.; Takayama, S. Fabrication of two-layered channel system with embedded electrodes to measure resistance across epithelial and endothelial barriers. *Anal. Chem.* **2010**, *82*, 2505–2511.
[51] Griep, L. M.;Wolbers, F.;de Wagenaar, B.;ter Braak, P. M.;Weksler, B. B.;Romero, I. A.;Couraud, P. O.;Vermes, I.;van der Meer, A. D.; van den Berg, A. BBB on chip: microfluidic platform to mechanically and biochemically modulate blood-brain barrier function. *Biomed. Microdevices* **2013**, *15*, 145–150.
[52] Nicolas, A.;Schavemaker, F.;Kosim, K.;Kurek, D.;Haarmans, M.;Bulst, M.;Lee, K.;Wegner, S.;Hankemeier, T.; Joore, J. High throughput transepithelial electrical resistance (TEER) measurements on perfused membrane-free epithelia. *Lab Chip* **2021**, *21*, 1676–1685.
[53] Wang, Y. I.;Abaci, H. E.; Shuler, M. L. Microfluidic blood–brain barrier model provides in vivo‐like barrier properties for drug permeability screening. *Biotechnol. Bioeng.* **2017**, *114*, 184–194.
[54] Kaden, T.;Besser, S.;Abdo, N.;Mosig, A. S.;Rennert, K.; Nietzsche, S. A plug-and-play transepithelial/transendothelial electric resistance (TEER)-upgraded organ-on-chip system to measure barrier dynamics in real-time. *bioRxiv* **2025**.
[55] Sei, Y. J.;Ahn, S. I.;Virtue, T.;Kim, T.; Kim, Y. Detection of frequency-dependent endothelial response to oscillatory shear stress using a microfluidic transcellular monitor. *Sci. Rep.* **2017**, *7*, 10019.
[56] Henry, O. Y.;Villenave, R.;Cronce, M. J.;Leineweber, W. D.;Benz, M. A.; Ingber, D. E. Organs-on-chips with integrated electrodes for trans-epithelial electrical resistance (TEER) measurements of human epithelial barrier function. *Lab Chip* **2017**, *17*, 2264–2271.
[57] Miyazaki, T.;Hirai, Y.;Kamei, K. i.;Tsuchiya, T.; Tabata, O. Design strategy of electrode patterns based on finite element analysis in microfluidic device for Trans‐Epithelial Electrical Resistance (TEER) measurement. *Electr. Commun. Jpn.* **2021**, *104*, e12296.
[58] Krishnakumar, A.;Kadian, S.;Heredia Rivera, U.;Chittiboyina, S.;Lelièvre, S. A.; Rahimi, R. Organ-on-a-chip platform with an integrated screen-printed electrode array for real-time monitoring trans-epithelial barrier and bubble formation. *ACS Biomater. Sci.*

Not Accepted

Eng. **2023**, *9*, 1620–1628.
[59] Matthiesen, I.;Voulgaris, D.;Nikolakopoulou, P.;Winkler, T. E.; Herland, A. Continuous monitoring reveals protective effects of N - acetylcysteine amide on an isogenic microphysiological model of the neurovascular unit. *Small* **2021**, *17*, 2101785.
[60] Yeste, J.;García-Ramírez, M.;Illa, X.;Guimerà, A.;Hernández, C.;Simó, R.; Villa, R. A compartmentalized microfluidic chip with crisscross microgrooves and electrophysiological electrodes for modeling the blood–retinal barrier. *Lab Chip* **2018**, *18*, 95–105.
[61] Fernandes, J.;Karra, N.;Bowring, J.;Reale, R.;James, J.;Blume, C.;Pell, T. J.;Rowan, W. C.;Davies, D. E.; Swindle, E. J. Real-time monitoring of epithelial barrier function by impedance spectroscopy in a microfluidic platform. *Lab Chip* **2022**, *22*, 2041–2054.
[62] Palma-Florez, S.;López-Canosa, A.;Moralez-Zavala, F.;Castaño, O.;Kogan, M. J.;Samitier, J.;Lagunas, A.; Mir, M. BBB-on-a-chip with integrated micro-TEER for permeability evaluation of multi-functionalized gold nanorods against Alzheimer's disease. *J. Nanobiotechnology* **2023**, *21*, 115.
[63] Ugodnikov, A.;Lu, J.;Yechuri, B.;Chebotarev, O.;Takeuchi, L. E.; Simmons, C. A. A Microfluidic Barrier-on-Chip Platform with Integrated Porous Membrane Cell–Substrate Impedance Spectroscopy. *ACS Appl. Mater. Interfaces* **2025**, *17*, 45398–45412.
[64] Lucchetti, M.;Werr, G.;Johansson, S.;Barbe, L.;Grandmougin, L.;Wilmes, P.; Tenje, M. Integration of multiple flexible electrodes for real-time detection of barrier formation with spatial resolution in a gut-on-chip system. *Microsyst. Nanoeng.* **2024**, *10*, 18.
[65] Onal, S.;Alkaisi, M. M.; Nock, V. Microdevice-based mechanical compression on living cells. *Iscience* **2022**, *25*, 105518.
[66] Perez Gonzalez, N.;Tao, J.;Rochman, N. D.;Vig, D.;Chiu, E.;Wirtz, D.; Sun, S. X. Cell tension and mechanical regulation of cell volume. *Mol. Biol. Cell* **2018**, *29*, 0.
[67] Tee, S.-Y.;Bausch, A. R.; Janmey, P. A. The mechanical cell. *Curr. Biol.* **2009**, *19*, R745–R748.
[68] Birukov, K. G. Cyclic stretch, reactive oxygen species, and vascular remodeling. *Antioxid. Redox. Signaling.* **2009**, *11*, 1651–1667.
[69] Münch, J.; Abdelilah-Seyfried, S. Sensing and responding of cardiomyocytes to changes of tissue stiffness in the diseased heart. *Front. Cell Dev. Biol.* **2021**, *9*, 642840.
[70] Janmey, P. A.;Fletcher, D. A.; Reinhart-King, C. A. Stiffness sensing by cells. *Physiol. Rev.* **2020**, *100*, 695–724.
[71] An, L.;Ji, F.;Zhao, E.;Liu, Y.; Liu, Y. Measuring cell deformation by microfluidics. *Front. Bioeng. Biotechnol.* **2023**, *11*, 1214544.
[72] Mermoud, Y.;Felder, M.;Stucki, J.;Stucki, A.; Guenat, O. Microimpedance tomography system to monitor cell activity and membrane movements in a breathing lung-on-chip. *Sens. Actuators B: Chem.* **2018**, *255*, 3647–3653.
[73] Kim, J.;Han, S.;Lei, A.;Miyano, M.;Bloom, J.;Srivastava, V.;Stampfer, M. R.;Gartner, Z. J.;LaBarge, M. A.; Sohn, L. L. Characterizing cellular mechanical phenotypes with mechano-node-pore sensing. *Microsyst. Nanoeng.* **2018**, *4*, 1–12.
[74] Liu, H.;MacQueen, L. A.;Usprech, J. F.;Maleki, H.;Sider, K. L.;Doyle, M. G.;Sun, Y.; Simmons, C. A. Microdevice arrays with strain sensors for 3D mechanical stimulation and monitoring of engineered tissues. *Biomaterials* **2018**, *172*, 30–40.
[75] Jayne, R. K.;Karakan, M. Ç.;Zhang, K.;Pierce, N.;Michas, C.;Bishop, D. J.;Chen, C. S.;Ekinci, K. L.; White, A. E. Direct laser writing for cardiac tissue engineering: a microfluidic heart on a chip with integrated transducers. *Lab Chip* **2021**, *21*, 1724–1737.
[76] Jin, Z. H.;Liu, Y. L.;Fan, W. T.; Huang, W. H. Integrating flexible electrochemical sensor into microfluidic chip for simulating and monitoring vascular mechanotransduction. *Small* **2020**, *16*, 1903204.
[77] Abaci, H. E.;Shen, Y. I.;Tan, S.; Gerecht, S. Recapitulating physiological and pathological shear stress and oxygen to model vasculature in health and disease. *Sci. Rep.* **2014**, *4*, 4951.
[78] Shemesh, J.;Jalilian, I.;Shi, A.;Heng Yeoh, G.;Knothe Tate, M. L.; Ebrahimi Warkiani, M. Flow-induced stress on adherent cells in microfluidic devices. *Lab Chip* **2015**, *15*, 4114–4127.
[79] Vasanthi Bathrinarayanan, P.;Abadie, T.;Perez Esteban, P.;Vigolo, D.;Simmons, M. J. H.; Grover, L. M. Elevated hydrostatic pressure destabilizes VE-cadherin junctions in a time and shear stress dependent manner: An endothelium-on-chip study. *APL Bioeng.* **2025**, *9*, 036113.
[80] Liu, M. C.;Shih, H. C.;Wu, J. G.;Weng, T. W.;Wu, C. Y.;Lu, J. C.; Tung, Y. C. Electrofluidic pressure sensor embedded microfluidic device: a study of endothelial cells under hydrostatic pressure and shear stress combinations. *Lab Chip* **2013**, *13*, 1743–1753.
[81] Wang, L.;Zhang, M.;Yang, M.;Zhu, W.;Wu, J.;Gong, X.; Wen, W. Polydimethylsiloxane-integratable micropressure sensor for microfluidic chips. *Biomicrofluidics* **2009**, *3*, 34105.
[82] Zarifi, M. H.;Sadabadi, H.;Hejazi, S. H.;Daneshmand, M.; Sanati-Nezhad, A. Noncontact and Nonintrusive Microwave-Microfluidic Flow Sensor for Energy and Biomedical Engineering. *Sci. Rep.* **2018**, *8*, 139.
[83] Islam, M. N.;Doria, S. M.;Fu, X.; Gagnon, Z. R. Piezoresistive Conductive Microfluidic Membranes for Low-Cost On-Chip Pressure and Flow Sensing. *Sensors* **2022**, *22*.
[84] Temiz, Y.; Delamarche, E. Sub-nanoliter, real-time flow monitoring in microfluidic chips using a portable device and smartphone. *Sci. Rep.* **2018**, *8*, 10603.
[85] Zhou, X.;Zhang, R.;Li, L.;Zhang, L.;Liu, B.;Deng, Z.;Wang, L.; Gui, L. A liquid metal based capacitive soft pressure microsensor. *Lab Chip* **2019**, *19*, 807–814.
[86] Huber, D.;Oskooei, A.;Casadevall, I. S. X.;Andrew, d.; Kaigala, G. V. Hydrodynamics in Cell Studies. *Chem. Rev.* **2018**, *118*, 2042–2079.
[87] Zhang, X.;Huk, D. J.;Wang, Q.;Lincoln, J.; Zhao, Y. A microfluidic shear device that accommodates parallel high and low stress zones within the same culturing chamber. *Biomicrofluidics* **2014**, *8*, 054106.
[88] Lin, Y. H.;Lau, S. F.;Lu, Y. P.;Huang, K. C.;Ding, C. F.;Tang, Y. H.; Tsai, H. Y. Biocompatible Heterogeneous Packaging and Laser-Assisted Fluid Interface Control for In Situ Sensor in Organ-on-a-Chip. *Micromachines* **2024**, *16*.
[89] Zhang, Z. J.;Hou, T.;Ren, Y.;Wang, C. B.;Wang, Z. K.;Pan, H.;Li, P. Y.;Smith, R.; Wang, J. Real-time embedded pressure and flow rate sensor in polydimethylsiloxane-based microchannel using fiber Bragg grating technique. *Flow Meas. Instrum.* **2024**, *96*.
[90] de Haan, P.;Mulder, J. P. S. H.;Lötters, J. C.; Verpoorte, E. A highly stable, pressure-driven, flow control system based on Coriolis mass flow sensors for organs-on-chips. *Flow Meas. Instrum.* **2024**, *97*.
[91] Vivas, A.;van den Berg, A.;Passier, R.;Odijk, M.; van der Meer, A. D. Fluidic circuit board with modular sensor and valves enables stand-alone, tubeless microfluidic flow control in organs-on-chips. *Lab Chip* **2022**, *22*, 1231–1243.
[92] Kieninger, J.;Weltin, A.;Flamm, H.; Urban, G. A. Microsensor systems for cell metabolism–from 2D culture to organ-on-chip. *Lab Chip* **2018**, *18*, 1274–1291.
[93] Coln, E.;Miller, C.;Hickman, J. J.; Long, C. J. Biosensor applications in organ-on-a-chip platforms and disease modeling. *Front. Bioeng. Biotechnol.* **2026**, *14*, 1824674.

Just Accepted

[94] Harriot, A. D.;Ward, C. W.; Kim, D. H. Microphysiological systems to advance human pathophysiology and translational medicine. *J. Appl. Physiol.* **2024**, *137*, 1494–1501.
[95] Cornish-Bowden, A. *Fundamentals of enzyme kinetics*; John Wiley & Sons: Weinheim, 2013.
[96] Cullis, P. R.;Hope, M. J.;Bally, M. B.;Madden, T. D.;Mayer, L. D.; Fenske, D. B. Influence of pH gradients on the transbilayer transport of drugs, lipids, peptides and metal ions into large unilamellar vesicles. *Biochim. Biophys. Acta Biomembr.* **1997**, *1331*, 187–211.
[97] Flinck, M.;Kramer, S.; Pedersen, S. Roles of pH in control of cell proliferation. *Acta Physiol.* **2018**, *223*, e13068.
[98] Lahiri, S. Historical perspectives of cellular oxygen sensing and responses to hypoxia. *J. Appl. Physiol.* **2000**, *88*, 1467–1473.
[99] Brennan, M. D.;Rexius-Hall, M. L.;Elgass, L. J.; Eddington, D. T. Oxygen control with microfluidics. *Lab Chip* **2014**, *14*, 4305–4318.
[100] Phypers, B.; Pierce, J. T. Lactate physiology in health and disease. *BJA Education* **2006**, *6*, 128–132.
[101] Kocianova, E.;Piatrikova, V.; Golias, T. Revisiting the Warburg effect with focus on lactate. *Cancers (Basel)* **2022**, *14*, 6028.
[102] Rothbauer, M.;Strauss, J.;Reihs, E. I.;Heidenberger, J.;Alphonsus, J.;Gowers, S.;Chen, Y.-C.;McLeod, J.;Toegel, S.; Ertl, P. Integration of glucose and lactate biosensors into human cartilage-on-a-chip models for long-term monitoring of metabolic shifts in osteoarthritis. *Sens. Actuators B: Chem.* **2025**, *427*, 137123.
[103] Veldhuizen, J.;Chavan, R.;Moghadas, B.;Park, J. G.;Kodibagkar, V. D.;Migrino, R. Q.; Nikkhah, M. Cardiac ischemia on-a-chip to investigate cellular and molecular response of myocardial tissue under hypoxia. *Biomaterials* **2022**, *281*, 121336.
[104] Sánchez-Salazar, M. G.;Garza-Garza, R.;Crespo-López Oliver, R.;Jerezano-Flores, V. S.;Gallegos-Martínez, S.;Ramos-Meizoso, S.;Verduzco-Valenzuela, M.;Trujillo-de Santiago, G.; Alvarez, M. M. Continuous inline monitoring of glucose in an organ-on-chip using FreeStyle™ libre glucometers. *Front. Lab Chip Technol.* **2024**, *3*, 1289437.
[105] Bauer, S.;Wennberg Huldt, C.;Kanebratt, K. P.;Durieux, I.;Gunne, D.;Andersson, S.;Ewart, L.;Haynes, W. G.;Maschmeyer, I.; Winter, A. Functional coupling of human pancreatic islets and liver spheroids on-a-chip: Towards a novel human ex vivo type 2 diabetes model. *Sci. Rep.* **2017**, *7*, 14620.
[106] Kieninger, J.;Aravindalochanan, K.;Sandvik, J.;Pettersen, E.; Urban, G. Pericellular oxygen monitoring with integrated sensor chips for reproducible cell culture experiments. *Cell Prolif.* **2014**, *47*, 180–188.
[107] Essaouiba, A.;Okitsu, T.;Kinoshita, R.;Jellali, R.;Shinohara, M.;Danoy, M.;Legallais, C.;Sakai, Y.; Leclerc, E. Development of a pancreas-liver organ-on-chip coculture model for organ-to-organ interaction studies. *Biochem. Eng. J.* **2020**, *164*, 107783.
[108] Zirath, H.;Spitz, S.;Roth, D.;Schellhorn, T.;Rothbauer, M.;Müller, B.;Walch, M.;Kaur, J.;Wörle, A.; Kohl, Y. Bridging the academic–industrial gap: application of an oxygen and pH sensor-integrated lab-on-a-chip in nanotoxicology. *Lab Chip* **2021**, *21*, 4237–4248.
[109] Lederle, M.;Tric, M.;Roth, T.;Schütte, L.;Rattenholl, A.;Lütkemeyer, D.;Wölfl, S.;Werner, T.; Wiedemann, P. Continuous optical in‐line glucose monitoring and control in CHO cultures contributes to enhanced metabolic efficiency while maintaining darbepoetin alfa product quality. *Biotechnol. J.* **2021**, *16*, 2100088.
[110] Müller, B.;Sulzer, P.;Walch, M.;Zirath, H.;Buryška, T.;Rothbauer, M.;Ertl, P.; Mayr, T. Measurement of respiration and acidification rates of mammalian cells in thermoplastic microfluidic devices. *Sens. Actuators B: Chem.* **2021**, *334*, 129664.
[111] Matsumoto, S.;Safitri, A. R.;Danoy, M.;Maekawa, T.;Kinoshita, H.;Shinohara, M.;Sakai, Y.;Fujii, T.; Leclerc, E. Investigation of the hepatic respiration and liver zonation on rat hepatocytes using an integrated oxygen biosensor in a microscale device. *Biotechnol. Prog.* **2019**, *35*, e2854.
[112] Lasave, L. C.;Borisov, S. M.;Ehgartner, J.; Mayr, T. Quick and simple integration of optical oxygen sensors into glass-based microfluidic devices. *RSC Adv.* **2015**, *5*, 70808–70816.
[113] Fuchs, S.;van Helden, R. W.;Wiendels, M.;de Graaf, M. N.;Orlova, V. V.;Mummery, C. L.;van Meer, B. J.; Mayr, T. On-chip analysis of glycolysis and mitochondrial respiration in human induced pluripotent stem cells. *Mater. Today Bio.* **2022**, *17*, 100475.
[114] Fuchs, S.;Rieger, V.;Tjell, A. Ø.;Spitz, S.;Brandauer, K.;Schaller-Ammann, R.;Feiel, J.;Ertl, P.;Klimant, I.; Mayr, T. Optical glucose sensor for microfluidic cell culture systems. *Biosens. Bioelectron.* **2023**, *237*, 115491.
[115] Zhang, Y. S.;Aleman, J.;Shin, S. R.;Kilic, T.;Kim, D.;Mousavi Shaegh, S. A.;Massa, S.;Riahi, R.;Chae, S.; Hu, N. Multisensor-integrated organs-on-chips platform for automated and continual in situ monitoring of organoid behaviors. *Proc. Natl. Acad. Sci. U. S. A.* **2017**, *114*, E2293–E2302.
[116] Gehre, C.;Flechner, M.;Kammerer, S.;Küpper, J.-H.;Coleman, C. D.;Püschel, G. P.;Uhlig, K.; Duschl, C. Real time monitoring of oxygen uptake of hepatocytes in a microreactor using optical microsensors. *Sci. Rep.* **2020**, *10*, 13700.
[117] Zirath, H.;Rothbauer, M.;Spitz, S.;Bachmann, B.;Jordan, C.;Müller, B.;Ehgartner, J.;Priglinger, E.;Mühleder, S.;Redl, H.;Holnthoner, W.;Harasek, M.;Mayr, T.; Ertl, P. Every Breath You Take: Non-invasive Real-Time Oxygen Biosensing in Two- and Three-Dimensional Microfluidic Cell Models. *Front. Physiol.* **2018**, *Volume 9 - 2018*, 815.
[118] Tanumihardja, E.;Rodríguez, A. P.;Loessberg-Zahl, J.;Mei, B.;Olthuis, W.; Van den Berg, A. On-chip electrocatalytic NO sensing using ruthenium oxide nanorods. *Sens. Actuators B: Chem.* **2021**, *334*, 129631.
[119] Tanumihardja, E.;Slaats, R. H.;van der Meer, A. D.;Passier, R.;Olthuis, W.; van den Berg, A. Measuring both pH and O2 with a single on-chip sensor in cultures of human pluripotent stem cell-derived cardiomyocytes to track induced changes in cellular metabolism. *ACS Sens.* **2020**, *6*, 267–274.
[120] Weltin, A.;Slotwinski, K.;Kieninger, J.;Moser, I.;Jobst, G.;Wego, M.;Ehret, R.; Urban, G. A. Cell culture monitoring for drug screening and cancer research: a transparent, microfluidic, multi-sensor microsystem. *Lab Chip* **2014**, *14*, 138–146.
[121] Misun, P. M.;Rothe, J.;Schmid, Y. R.;Hierlemann, A.; Frey, O. Multi-analyte biosensor interface for real-time monitoring of 3D microtissue spheroids in hanging-drop networks. *Microsyst. Nanoeng.* **2016**, *2*, 1–9.
[122] Dornhof, J.;Kieninger, J.;Muralidharan, H.;Maurer, J.;Urban, G. A.; Weltin, A. Microfluidic organ-on-chip system for multi-analyte monitoring of metabolites in 3D cell cultures. *Lab Chip* **2022**, *22*, 225–239.
[123] Su, S. H.;Song, Y.;Stephens, A.;Situ, M.;McCloskey, M. C.;McGrath, J. L.;Andjelkovic, A. V.;Singer, B. H.; Kurabayashi, K. A tissue chip with integrated digital immunosensors: In situ brain endothelial barrier cytokine secretion monitoring. *Biosens. Bioelectron.* **2023**, *224*, 115030.
[124] Batista Napotnik, T.;Cimperman, T.; Rems, L. Excitation and electroporation in genetically engineered excitable S-HEK cells exposed to electric pulses of different durations. *Sci. Rep.* **2025**, *15*, 23451.
[125] Liu, H.;Bolonduro, O. A.;Hu, N.;Ju, J.;Rao, A. A.;Duffy, B. M.;Huang, Z.;Black, L. D.; Timko, B. P. Heart-on-a-chip model with

Just Accepted

integrated extra-and intracellular bioelectronics for monitoring cardiac electrophysiology under acute hypoxia. *Nano Lett.* **2020**, *20*, 2585–2593.
[126] Lewandowska, M. K.;Bakkum, D. J.;Rompani, S. B.; Hierlemann, A. Recording large extracellular spikes in microchannels along many axonal sites from individual neurons. *PLoS One* **2015**, *10*, e0118514.
[127] Perrier, R.;Pirog, A.;Jaffredo, M.;Gaitan, J.;Catargi, B.;Renaud, S.;Raoux, M.; Lang, J. Bioelectronic organ-based sensor for microfluidic real-time analysis of the demand in insulin. *Biosens. Bioelectron.* **2018**, *117*, 253–259.
[128] Obien, M. E. J.;Deligkaris, K.;Bullmann, T.;Bakkum, D. J.; Frey, U. Revealing neuronal function through microelectrode array recordings. *Front. Neurosci.* **2015**, *8*, 423.
[129] Kumar, P.;Si, M.;Paulhus, K.; Glasscock, E. Microelectrode array recording of sinoatrial node firing rate to identify intrinsic cardiac pacemaking defects in mice. *J. Vis. Exp.* **2021**, 10.3791/62735.
[130] Park, M. U.;Bae, Y.;Lee, K.-S.;Song, J. H.;Lee, S.-M.; Yoo, K.-H. Collective dynamics of neuronal activities in various modular networks. *Lab Chip* **2021**, *21*, 951–961.
[131] Ye, Y.;Wan, S.;Li, S.;Peng, Y.;He, X.; Qin, M. Fabrication and characterization of a MEMS thermal convective accelerometer on silicon-in-glass substrate. *IEEE Sens. J.* **2024**, *24*, 9619–9625.
[132] Lee, Y.-C.;Wang, L.-K.;Chuang, Y.-C.;Hong, H.-C.; Chiu, Y. Electrothermal tunable MEMS oscillators for MEMS-based reservoir computing. *IEEE Sens. Lett.* **2024**, *8*, 1–4.
[133] Padha, B.;Yadav, I.;Dutta, S.; Arya, S. Recent developments in wearable NEMS/MEMS-based smart infrared sensors for healthcare applications. *ACS Appl. Electron. Mater.* **2023**, *5*, 5386–5411.
[134] Khan, A. A.;Nguyen, T.-K.;Trinh, Q. T.;Nguyen, N.-T.;Dao, D. V.; Zhu, Y. Wafer Bonding Technologies for Microelectromechanical Systems and 3D ICs: Advances, Challenges, and Trends. *Adv. Eng. Mater.* **2025**, *27*, 2500342.
[135] Karimzadehkhouei, M.;Ali, B.;Jedari Ghourichaei, M.; Alaca, B. E. Silicon nanowires driving miniaturization of microelectromechanical systems physical sensors: A review. *Adv. Eng. Mater.* **2023**, *25*, 2300007.
[136] Dong, Z.;He, Q.;Shen, D.;Gong, Z.;Zhang, D.;Zhang, W.;Ono, T.; Jiang, Y. Microfabrication of functional polyimide films and microstructures for flexible MEMS applications. *Microsyst. Nanoeng.* **2023**, *9*, 31.
[137] Li, R.;Wang, Z.;He, L.;Wang, B.;Mao, H.; Yu, M. Characterization of the effect of fractal micro-protrusion and heat on the wettability behavior on chips in medical MEMS. *Mater. Today Commun.* **2024**, *39*, 108547.
[138] Ling, H.-D.;Luo, Y.-D.;Xu, G.-J.;He, Y.-Z.;Xu, S.-T.;Ma, R.-D.; Cao, H.-Z. An easily available and flexible fabrication protocol for microstructures by using printed mask projection lithography and silver mirror reaction. *Micro Nanostructures* **2025**, *205*, 208170.
[139] Wang, P.;Ma, X.;Lin, Z.;Chen, F.;Chen, Z.;Hu, H.;Xu, H.;Zhang, X.;Shi, Y.; Huang, Q. Well-defined in-textile photolithography towards permeable textile electronics. *Nat. Commun.* **2024**, *15*, 887.
[140] Feng, F.;Liu, Y.;Zhang, K.;Yang, H.;Hyun, B.-R.;Xu, K.;Kwok, H.-S.; Liu, Z. High-power AlGaN deep-ultraviolet micro-light-emitting diode displays for maskless photolithography. *Nat. Photon.* **2025**, *19*, 101–108.
[141] Kang, S.-H.;Jo, J.-W.;Lee, J. M.;Moon, S.;Shin, S. B.;Choi, S. B.;Byeon, D.;Kim, J.;Kim, M.-G.; Kim, Y.-H. Full integration of highly stretchable inorganic transistors and circuits within molecular-tailored elastic substrates on a large scale. *Nat. Commun.* **2024**, *15*, 2814.
[142] Yang, Y.;Dai, Z.;Chen, Y.;Yuan, Y.;Yalikun, Y.; Shang, C. Emerging MEMS sensors for ocean physics: Principles, materials, and applications. *Appl. Phys. Rev.* **2024**, *11*.
[143] Gubbi, V.;Ivanov, T.;Ved, K.;Lenk, C.; Ziegler, M. Bio-inspired acoustic MEMS sensor with tunable resonance frequency. *Sens. Actuators A: Phys.* **2025**, *387*, 116369.
[144] Priya, S.;Mohan, S.;Kuppusamy, R.;Suyambulingam, I.;Baby, B.;Ramesh, R.; Han, S. S. Advances in Bio-Microelectromechanical System-Based Sensors for Next-Generation Healthcare Applications. *ACS omega* **2025**, *10*, 34088–34105.
[145] Ahmad, M.;Bahri, M.; Sawan, M. MEMS Micromirror Actuation Techniques: A Comprehensive Review of Trends, Innovations, and Future Prospects. *Micromachines* **2024**, *15*, 1233.
[146] Ba Hashwan, S. S.;Khir, M. H. M.;Nawi, I. M.;Ahmad, M. R.;Hanif, M.;Zahoor, F.;Al-Douri, Y.;Algamili, A. S.;Bature, U. I.; Alabsi, S. S. A review of piezoelectric MEMS sensors and actuators for gas detection application. *Discov. Nano.* **2023**, *18*, 25.
[147] Choi, D.;Park, Y. J.;Her, M. J.; Han, S. MEMS Actuators for Tunable Waveguide Devices in Photonic Integrated Circuits: A Brief Review. *Curr. Opt. Photon.* **2025**, *9*, 185–195.
[148] Mahmud, M. P.;Bazaz, S. R.;Dabiri, S.;Mehrizi, A. A.;Asadnia, M.;Warkiani, M. E.; Wang, Z. L. Advances in mems and microfluidics‐based energy harvesting technologies. *Adv. Mater. Technol.* **2022**, *7*, 2101347.
[149] Naghib, S. M.; Rezaeian, Y. Microfluidic Micropumps: Advancing Biomedical Applications with Micro Electromechanical-Based Systems (MEMS). In *Frontiers of Nanobiotechnology: Microfluidic Devices and BioMEMS for the Future*. Springer; Cham, 2025; pp 93–135.
[150] Renous, N.;Kiri, M. D.;Barnea, R. A.;Rauti, R.;Leichtmann-Bardoogo, Y.; Maoz, B. M. Spatial trans-epithelial electrical resistance (S-TEER) integrated in organs-on-chips. *Lab Chip* **2022**, *22*, 71–79.
[151] Booth, R.; Kim, H. Characterization of a microfluidic in vitro model of the blood-brain barrier (μBBB). *Lab Chip* **2012**, *12*, 1784–1792.
[152] van der Helm, M. W.;Henry, O. Y.;Bein, A.;Hamkins-Indik, T.;Cronce, M. J.;Leineweber, W. D.;Odijk, M.;van der Meer, A. D.;Eijkel, J. C.; Ingber, D. E. Non-invasive sensing of transepithelial barrier function and tissue differentiation in organs-on-chips using impedance spectroscopy. *Lab Chip* **2019**, *19*, 452–463.
[153] Aleman, J.;Kilic, T.;Mille, L. S.;Shin, S. R.; Zhang, Y. S. Microfluidic integration of regeneratable electrochemical affinity-based biosensors for continual monitoring of organ-on-a-chip devices. *Nat. Protoc.* **2021**, *16*, 2564–2593.
[154] Elhami Nik, F.;Matthiesen, I.;Herland, A.; Winkler, T. E. Low-Cost PVD Shadow Masks with Submillimeter Resolution from Laser-Cut Paper. *Micromachines* **2020**, *11*.
[155] Maoz, B. M.;Herland, A.;Henry, O. Y.;Leineweber, W. D.;Yadid, M.;Doyle, J.;Mannix, R.;Kujala, V. J.;FitzGerald, E. A.; Parker, K. K. Organs-on-Chips with combined multi-electrode array and transepithelial electrical resistance measurement capabilities. *Lab Chip* **2017**, *17*, 2294–2302.
[156] Wong, J. F.;Mohan, M. D.;Young, E. W.; Simmons, C. A. Integrated electrochemical measurement of endothelial permeability in a 3D hydrogel-based microfluidic vascular model. *Biosens. Bioelectron.* **2020**, *147*, 111757.
[157] Quirós-Solano, W. F.;Gaio, N.;Silvestri, C.;Pandraud, G.;Dekker, R.; Sarro, P. M. Metal and polymeric strain gauges for Si-based,
Just Accepted

monolithically fabricated organs-on-chips. *Micromachines* **2019**, *10*, 536.
[158] Zhang, X.;Wang, W.;Li, F.; Voiculescu, I. Stretchable impedance sensor for mammalian cell proliferation measurements. *Lab Chip* **2017**, *17*, 2054–2066.
[159] Tran, T. B.;Baek, C.; Min, J. Electric cell-substrate impedance sensing (ECIS) with microelectrode arrays for investigation of cancer cell–fibroblasts interaction. *PLoS One* **2016**, *11*, e0153813.
[160] Oleaga, C.;Riu, A.;Rothemund, S.;Lavado, A.;McAleer, C. W.;Long, C. J.;Persaud, K.;Narasimhan, N. S.;Tran, M.; Roles, J. Investigation of the effect of hepatic metabolism on off-target cardiotoxicity in a multi-organ human-on-a-chip system. *Biomaterials* **2018**, *182*, 176–190.
[161] Aydogmus, H.;Hu, M.;Ivancevic, L.;Frimat, J.-P.;van den Maagdenberg, A. M.;Sarro, P. M.; Mastrangeli, M. An organ-on-chip device with integrated charge sensors and recording microelectrodes. *Sci. Rep.* **2023**, *13*, 8062.
[162] da Ponte, R. M.;Gaio, N.;van Zeijl, H.;Vollebregt, S.;Dijkstra, P.;Dekker, R.;Serdijn, W. A.; Giagka, V. Monolithic integration of a smart temperature sensor on a modular silicon-based organ-on-a-chip device. *Sens. Actuators A: Phys.* **2021**, *317*, 112439.
[163] Moya, A.;Ortega-Ribera, M.;Guimerà, X.;Sowade, E.;Zea, M.;Illa, X.;Ramon, E.;Villa, R.;Gracia-Sancho, J.; Gabriel, G. Online oxygen monitoring using integrated inkjet-printed sensors in a liver-on-a-chip system. *Lab Chip* **2018**, *18*, 2023–2035.
[164] Kawakita, S.;Li, S.;Nguyen, H. T.;Maity, S.;Haghniaz, R.;Bahari, J.;Yu, N.;Mandal, K.;Bandaru, P.; Mou, L. Rapid integration of screen-printed electrodes into thermoplastic organ-on-a-chip devices for real-time monitoring of trans-endothelial electrical resistance. *Biomed. Microdevices* **2023**, *25*, 37.
[165] Khalid, M. A. U.;Kim, K. H.;Salih, A. R. C.;Hyun, K.;Park, S. H.;Kang, B.;Soomro, A. M.;Ali, M.;Jun, Y.; Huh, D. High performance inkjet printed embedded electrochemical sensors for monitoring hypoxia in a gut bilayer microfluidic chip. *Lab Chip* **2022**, *22*, 1764–1778.
[166] Ehgartner, J.;Sulzer, P.;Burger, T.;Kasjanow, A.;Bouwes, D.;Krühne, U.;Klimant, I.; Mayr, T. Online analysis of oxygen inside silicon-glass microreactors with integrated optical sensors. *Sens. Actuators B: Chem.* **2016**, *228*, 748–757.
[167] Lind, J. U.;Busbee, T. A.;Valentine, A. D.;Pasqualini, F. S.;Yuan, H.;Yadid, M.;Park, S.-J.;Kotikian, A.;Nesmith, A. P.; Campbell, P. H. Instrumented cardiac microphysiological devices via multimaterial three-dimensional printing. *Nat. Mater.* **2017**, *16*, 303–308.
[168] Wu, Q.;Xue, R.;Zhao, Y.;Ramsay, K.;Wang, E. Y.;Savoji, H.;Veres, T.;Cartmell, S. H.; Radisic, M. Automated fabrication of a scalable heart-on-a-chip device by 3D printing of thermoplastic elastomer nanocomposite and hot embossing. *Bioact. Mater.* **2024**, *33*, 46–60.
[169] Kim, E.;Park, W.;Hong, Y. M.;Hong, J.;Jeong, I.;Lee, J.;Lee, S.;Lee, H.;Kim, H. M.;Wulansari, N.;Hwang, D. Y.; Park, J. U. Neural dynamics of temporal interference stimulation monitoring by soft liquid metal interfaces across neural systems. *Nat. Commun.* **2026**, *17*.
[170] Kim, E.;Jeong, E.;Hong, Y. M.;Jeong, I.;Kim, J.;Kwon, Y. W.;Park, Y. G.;Lee, J.;Choi, S.;Kim, J. Y.;Lee, J. H.;Cho, S. W.; Park, J. U. Magnetically reshapable 3D multi-electrode arrays of liquid metals for electrophysiological analysis of brain organoids. *Nat. Commun.* **2025**, *16*, 2011.
[171] Marrero, D.;Pujol-Vila, F.;Tuset, E.;Gabriel, G.;Villa, R.;Alvarez, M.; Illa, X. Low-temperature inkjet-printed electrochemical sensors on OSTE+ microfluidics for oxygen monitoring and scavenging. *Lab Chip* **2026**, *26*, 2775–2788.
[172] Kopic, I.;Peng, H.;Schmidt, S.;Berezin, O.;Wang, S.;Westmeyer, G. G.; Wolfrum, B. Inkjet-Printed 3D Sensor Arrays with FIB-Induced Electrode Refinement for Low-Noise Amperometric Recordings in hiPSC-Derived Brain Organoids. *ACS Sens.* **2025**, *10*, 6426–6435.
[173] Guo, Y.;Patanwala, H. S.;Bognet, B.; Ma, A. W. Inkjet and inkjet-based 3D printing: connecting fluid properties and printing performance. *Rapid Prototyp. J.* **2017**, *23*, 562–576.
[174] Batine, A.;Boumegnane, A.;Nadi, A.;Cochrane, C.;Cherkaoui, O.; Tahiri, M. Advances in Screen‐Printed Conductive Inks for Sustainable and High‐Performance E‐Textiles: Innovations, Challenges, and Future Prospects. *Adv. Eng. Mater.* **2025**, *27*, 2501322.
[175] Chen, C.;Ran, C.;Yao, Q.;Wang, J.;Guo, C.;Gu, L.;Han, H.;Wang, X.;Chao, L.; Xia, Y. Screen‐printing technology for scale manufacturing of perovskite solar cells. *Adv. Sci.* **2023**, *10*, 2303992.
[176] Zavanelli, N.; Yeo, W.-H. Advances in screen printing of conductive nanomaterials for stretchable electronics. *ACS omega* **2021**, *6*, 9344–9351.
[177] Orzari, L. O.;Kalinke, C.;Silva-Neto, H. A.;Rocha, D. S.;Camargo, J. R.;Coltro, W. K.; Janegitz, B. C. Screen-printing vs additive manufacturing approaches: recent aspects and trends involving the fabrication of electrochemical sensors. *Anal. Chem.* **2025**, *97*, 1482–1494.
[178] Rennert, K.;Steinborn, S.;Gröger, M.;Ungerböck, B.;Jank, A.-M.;Ehgartner, J.;Nietzsche, S.;Dinger, J.;Kiehntopf, M.;Funke, H.;Peters, F. T.;Lupp, A.;Gärtner, C.;Mayr, T.;Bauer, M.;Huber, O.; Mosig, A. S. A microfluidically perfused three dimensional human liver model. *Biomaterials* **2015**, *71*, 119–131.
[179] Mousavi Shaegh, S. A.;De Ferrari, F.;Zhang, Y. S.;Nabavinia, M.;Binth Mohammad, N.;Ryan, J.;Pourmand, A.;Laukaitis, E.;Banan Sadeghian, R.; Nadhman, A. A microfluidic optical platform for real-time monitoring of pH and oxygen in microfluidic bioreactors and organ-on-chip devices. *Biomicrofluidics* **2016**, *10*, 044111.
[180] Azimzadeh, M.;Khashayar, P.;Amereh, M.;Tasnim, N.;Hoorfar, M.; Akbari, M. Microfluidic-based oxygen (O2) sensors for on-chip monitoring of cell, tissue and organ metabolism. *Biosensors* **2021**, *12*, 6.
[181] Kratz, S.;Höll, G.;Schuller, P.;Ertl, P.; Rothbauer, M. Latest Trends in Biosensing for Microphysiological Organs-on-a-Chip and Body-on-a-Chip Systems. *Biosensors* **2019**, *9*.
[182] Liu, Y.;Liu, Y.;Matharu, Z.;Rahimian, A.; Revzin, A. Detecting multiple cell-secreted cytokines from the same aptamer-functionalized electrode. *Biosens. Bioelectron.* **2015**, *64*, 43–50.
[183] Zhang, J.;Cheng, Z.;Li, P.; Tian, B. Materials and device strategies to enhance spatiotemporal resolution in bioelectronics. *Nat. Rev. Mater.* **2025**, *10*, 425–448.
[184] Schröter, M.;Cardes, F.;Bui, C.-V. H.;Dodi, L. D.;Gänswein, T.;Bartram, J.;Sadiraj, L.;Hornauer, P.;Kumar, S.;Pascual-Garcia, M.; Hierlemann, A. Advances in large-scale electrophysiology with high-density microelectrode arrays. *Lab Chip* **2025**, *25*, 4844–4885.
[185] Bergamini, C. M.;Gambetti, S.;Dondi, A.; Cervellati, C. Oxygen, reactive oxygen species and tissue damage. *Curr. Pharm. Des.* **2004**, *10*, 1611–1626.
[186] Schneider, O.;Moruzzi, A.;Fuchs, S.;Grobel, A.;Schulze, H. S.;Mayr, T.; Loskill, P. Fusing spheroids to aligned μ-tissues in a heart-

Just Accepted

on-chip featuring oxygen sensing and electrical pacing capabilities. *Mater. Today Bio.* **2022**, *15*, 100280.
[187] Yeste, J.;Illa, X.;Guimerà, A.; Villa, R. A novel strategy to monitor microfluidic in-vitro blood-brain barrier models using impedance spectroscopy. In *Bio-MEMS and Medical Microdevices II*; SPIE; Barcelona, Spain, 2015; pp 123–128.
[188] Ishai, P. B.;Talary, M. S.;Caduff, A.;Levy, E.; Feldman, Y. Electrode polarization in dielectric measurements: a review. *Meas. Sci. Technol.* **2013**, *24*, 102001.
[189] Pranti, A. S.;Schander, A.;Bödecker, A.; Lang, W. PEDOT: PSS coating on gold microelectrodes with excellent stability and high charge injection capacity for chronic neural interfaces. *Sens. Actuators B: Chem.* **2018**, *275*, 382–393.
[190] Wisniewski, N.;Moussy, F.; Reichert, W. Characterization of implantable biosensor membrane biofouling. *Fresenius J. Anal. Chem.* **2000**, *366*, 611–621.
[191] Jiang, C.;Wang, G.;Hein, R.;Liu, N.;Luo, X.; Davis, J. J. Antifouling strategies for selective in vitro and in vivo sensing. *Chem. Rev.* **2020**, *120*, 3852–3889.
[192] Giménez-Gómez, P.;Rodríguez-Rodríguez, R.;Ríos, J. M.;Pérez-Montero, M.;González, E.;Gutiérrez-Capitán, M.;Plaza, J. A.;Muñoz-Berbel, X.; Jiménez-Jorquera, C. A self-calibrating and multiplexed electrochemical lab-on-a-chip for cell culture analysis and high-resolution imaging. *Lab Chip* **2020**, *20*, 823–833.
[193] Steinegger, A.;Wolfbeis, O. S.; Borisov, S. M. Optical sensing and imaging of pH values: Spectroscopies, materials, and applications. *Chem. Rev.* **2020**, *120*, 12357–12489.
[194] Chen, L.;Shinha, K.;Nakamura, H.;Komori, K.; Kimura, H. A Microfluidic Device Integrating a Glucose Sensor and Calibration Function for Cell-Based Assays. *Biosensors* **2025**, *15*.
[195] Prill, S.;Jaeger, M. S.; Duschl, C. Long-term microfluidic glucose and lactate monitoring in hepatic cell culture. *Biomicrofluidics* **2014**, *8*.
[196] Kumar, P.;Ravikumar, H.;Awasthi, A.;Raghunathan, M.; Kapoor, A. Sustainable paper-based platforms for cellular studies: A review. *Microchem. J.* **2025**, *212*, 113409.
[197] Lee, J.;Maji, S.; Lee, H. Fabrication and integration of a low‐cost 3D printing‐based glucose biosensor for bioprinted liver‐on‐a‐chip. *Biotechnol. J.* **2023**, *18*, 2300154.
[198] Ferrari, E.;Palma, C.;Vesentini, S.;Occhetta, P.; Rasponi, M. Integrating Biosensors in Organs-on-Chip Devices: A Perspective on Current Strategies to Monitor Microphysiological Systems. *Biosensors* **2020**, *10*.
[199] Izadifar, Z.;Charrez, B.;Almeida, M.;Robben, S.;Pilobello, K.;van der Graaf-Mas, J.;Marquez, S. L.;Ferrante, T. C.;Shcherbina, K.;Gould, R.;LoGrande, N. T.;Sesay, A. M.; Ingber, D. E. Organ chips with integrated multifunctional sensors enable continuous metabolic monitoring at controlled oxygen levels. *Biosens. Bioelectron.* **2024**, *265*.
[200] Kim, M.;Hwang, J. C.;Min, S.;Park, Y.-G.;Kim, S.;Kim, E.;Seo, H.;Chung, W. G.;Lee, J.;Cho, S.-W.; Park, J.-U. Multimodal Characterization of Cardiac Organoids Using Integrations of Pressure-Sensitive Transistor Arrays with Three-Dimensional Liquid Metal Electrodes. *Nano Lett.* **2022**, *22*, 7892–7901.
[201] Young, A. T.;Rivera, K. R.;Erb, P. D.; Daniele, M. A. Monitoring of Microphysiological Systems: Integrating Sensors and Real-Time Data Analysis toward Autonomous Decision-Making. *ACS Sens.* **2019**, *4*, 1454–1464.
[202] Li, J.;Xin, J.;Qu, L.;Xu, L.;Huang, Y.;Gu, Z.;Qi, L.-W.; Wang, Z. Artificial intelligence across organ-on-a-chip workflows: current implementations and future approaches. *Biofabrication* **2026**.
[203] Han, S.;Kim, T.;Kim, D.;Park, Y.-L.; Jo, S. Use of deep learning for characterization of microfluidic soft sensors. *IEEE Robot. Autom. Lett.* **2018**, *3*, 873–880.
[204] Kim, D.;Lee, S.;Kim, S.;Noh, Y.;Yeom, E.; Ahn, S. I. Learning-aided design of micropost arrays for optimizing interface stability and mass transport in organs-on-chips. *Lab Chip* **2026**.
[205] McIntyre, D.;Lashkaripour, A.;Fordyce, P.; Densmore, D. Machine learning for microfluidic design and control. *Lab Chip* **2022**, *22*, 2925–2937.
[206] Bocan, A.;Siavash Moakhar, R.;del Real Mata, C.;Petkun, M.;De Iure‐Grimmel, T.;Yedire, S. G.;Shieh, H.;Khorrami Jahromi, A.;Mahshid, S. S.; Mahshid, S. Machine‐Learning‐Aided Advanced Electrochemical Biosensors. *Adv. Mater.* **2025**, *37*, 2417520.
[207] Wang, H.;Wang, Y.; Xiong, S. Data Analysis and Prediction of Electrochemical Properties of Carbon Nanomaterials Based on Machine Learning. In *International Conference on Machine Learning, Image Processing, Network Security and Data Sciences*; Springer; Bhopal, India, 2022; pp 345–352.
[208] Li, A.;Yang, H.;Yu, W.;Liu, T.;Luo, B.; Zhao, C. Application of machine learning to improve the accuracy of electrochemical sensors: A review. *TrAC - Trends Anal. Chem.* **2025**, *193*.
[209] Giordano, G. F.;Ferreira, L. F.;Bezerra, Í. R. S.;Barbosa, J. A.;Costa, J. N. Y.;Pimentel, G. J. C.; Lima, R. S. Machine learning toward high-performance electrochemical sensors. *Analytical and Bioanalytical Chemistry* **2023**, *415*, 3683–3692.
[210] Zhang, B.;Zhang, Y.;Shen, J.;Zhou, Z.; Zhu, G. Research on differential pulse voltammetry detection method for low concentration glucose based on machine learning model. *International Journal of Electrochemical Science* **2024**, *19*.
[211] Aiassa, S.;Ny Hanitra, I.;Sandri, G.;Totu, T.;Grassi, F.;Criscuolo, F.;De Micheli, G.;Carrara, S.; Demarchi, D. Continuous monitoring of propofol in human serum with fouling compensation by support vector classifier. *Biosens. Bioelectron.* **2021**, *171*.
[212] de Oliveira Filho, J. I.;Faleiros, M. C.;Ferreira, D. C.;Mani, V.; Salama, K. N. Empowering Electrochemical Biosensors with AI: Overcoming Interference for Precise Dopamine Detection in Complex Samples. *Advanced Intelligent Systems* **2023**, *5*.
[213] Han, J.;Xu, X.;Li, J.;Zhang, H.;Su, W.;Wang, K.;Li, H.;Xu, Z.;Chen, J.;Cai, X.;Sun, Y.; Wang, L. Mechanically Matched Heart-on-a-Chip Platform Mediated Maturation of Excitation–Contraction Coupling. *ACS Nano* **2025**, *19*, 24052–24066.
[214] Tak, S.;Han, G.;Leem, S.-H.;Lee, S.-Y.;Paek, K.; Kim, J. A. Prediction of anticancer drug resistance using a 3D microfluidic bladder cancer model combined with convolutional neural network-based image analysis. *Front. Bioeng. Biotechnol.* **2024**, *11*.
[215] Han, X.;Matsuda, N.;Yamanaka, M.; Suzuki, I. Development of a Novel Microphysiological System for Peripheral Neurotoxicity Prediction Using Human iPSC-Derived Neurons with Morphological Deep Learning. *Toxics* **2024**, *12*.
[216] Ibrahim, M. S.; Kim, M. Artificial Intelligence-Aided Microfluidic Cell Culture Systems. *Biosensors* **2025**, *16*.
[217] Nakata, S.;Arie, T.;Akita, S.; Takei, K. Wearable, flexible, and multifunctional healthcare device with an ISFET chemical sensor for simultaneous sweat pH and skin temperature monitoring. *ACS Sens.* **2017**, *2*, 443–448.
[218] Xu, K.;Lu, Y.; Takei, K. Multifunctional skin‐inspired flexible sensor systems for wearable electronics. *Adv. Mater. Technol.* **2019**, *4*, 1800628.
[219] Khan, Y.;Thielens, A.;Muin, S.;Ting, J.;Baumbauer, C.; Arias, A. C. A new frontier of printed electronics: flexible hybrid

Accepted

electronics. *Adv. Mater.* **2020**, *32*, 1905279.
[220] Pan, J. Y.;Rezaei, B.;Anhøj, T. A.;Larsen, N. B.; Keller, S. S. Hybrid microfabrication of 3D pyrolytic carbon electrodes by photolithography and additive manufacturing. *Micro Nano Eng.* **2022**, *15*, 100124.
[221] Du, Y.;Reitemeier, J.;Jiang, Q.;Bappy, M. O.;Bohn, P. W.; Zhang, Y. Hybrid printing of fully integrated microfluidic devices for biosensing. *Small* **2024**, *20*, 2304966.
[222] Promphet, N.;Thanawattano, C.;Buekban, C.;Laochai, T.;Lormaneenopparat, P.;Sukmas, W.;Rattanawaleedirojn, P.;Puthongkham, P.;Potiyaraj, P.; Leewattanakit, W. Smartphone based wearable sweat glucose sensing device correlated with machine learning for real-time diabetes screening. *Anal. Chim. Acta* **2024**, *1312*, 342761.
[223] Wu, Q.;Zhang, P.;O'Leary, G.;Zhao, Y.;Xu, Y.;Rafatian, N.;Okhovatian, S.;Landau, S.;Valiante, T. A.;Travas-Sejdic, J.; Radisic, M. Flexible 3D printed microwires and 3D microelectrodes for heart-on-a-chip engineering. *Biofabrication* **2023**, *15*.
[224] Pourmostafa, A.;Bhusal, A.;Haridas Menon, N.;Li, Z.;Basuray, S.; Miri, A. K. Integrating conductive electrodes into hydrogel-based microfluidic chips for real-time monitoring of cell response. *Front. Bioeng. Biotechnol.* **2024**, *12*, 1421592.
[225] Tomaskovic-Crook, E.;Zhang, P.;Ahtiainen, A.;Kaisvuo, H.;Lee, C. Y.;Beirne, S.;Aqrawe, Z.;Svirskis, D.;Hyttinen, J.;Wallace, G. G.;Travas-Sejdic, J.; Crook, J. M. Human Neural Tissues from Neural Stem Cells Using Conductive Biogel and Printed Polymer Microelectrode Arrays for 3D Electrical Stimulation. *Adv. Healthc. Mater.* **2019**, *8*, e1900425.
[226] Perottoni, S.;Bonacina, A.;Dell'Oro, R.;Boeri, L.;Donnaloja, F.;Magagnin, L.;Petrini, P.;Albani, D.; Giordano, C. Sensors Manufacturing on a 3D-Printed Transwell-Based Hybrid Organ-on-a-Chip for Non-Invasive Real-Time Biological Barrier Resistance Monitoring. *ACS Biomater. Sci. Eng.* **2025**, *11*, 7570–7581.

Just Accepted